










## Open Archive Toulouse Archive Ouverte (OATAO)

OATAO is an open access repository that collects the work of Toulouse researchers and makes it freely available over the web where possible

This is an author's version published in: <http://oatao.univ-toulouse.fr/27593>

**Official URL:** <https://doi.org/10.1039/d0ce00132e>

### To cite this version:

Mayen, Laëtitia  and Jensen, Nicholai D. and Desbord, Maximilien  and Laurencin, Danielle and Gervais, Christel and Bonhomme, Christian and Smith, Mark E. and Porcher, Florence and Elkaim, Erik and Charvillat, Cédric  and Gras, Pierre  and Rey, Christian  and Soulié, Jérémy  and Combes, Christèle  *Advances in the synthesis and structure of  $\alpha$ -canaphite: a multitool and multiscale study.* (2020) CrystEngComm, 22 (18). 3130-3143. ISSN 1466-8033

Any correspondence concerning this service should be sent to the repository administrator: [tech-oatao@listes-diff.inp-toulouse.fr](mailto:tech-oatao@listes-diff.inp-toulouse.fr)

# Advances in the synthesis and structure of $\alpha$ -canaphite: a multitool and multiscale study†

Laëtitia Mayen,<sup>a</sup> Nicholai D. Jensen,<sup>bc</sup> Maximilien Desbord,<sup>a</sup> Danielle Laurencin,<sup>id b</sup> Christel Gervais,<sup>id c</sup> Christian Bonhomme,<sup>id c</sup> Mark E. Smith,<sup>id def</sup> Florence Porcher,<sup>g</sup> Erik Elkaim,<sup>h</sup> Cédric Charvillat,<sup>a</sup> Pierre Gras,<sup>a</sup> Christian Rey,<sup>a</sup> Jérémy Soulié<sup>id a</sup> and Christèle Combes<sup>id \*a</sup>

$\alpha$ -Canaphite ( $\text{CaNa}_2\text{P}_2\text{O}_7 \cdot 4\text{H}_2\text{O}$ ) is a layered calcium disodium pyrophosphate tetrahydrate phase of significant geological and potential biological interest. This study overcomes the lack of a reliable protocol to synthesize pure  $\alpha$  canaphite by using a novel simple and reproducible approach of double decomposition in solution at room temperature. The pure  $\alpha$ -canaphite is then characterized from the atomic to the macroscopic level using a multitool and multiscale advanced characterization strategy, providing for the first time full resolution of the  $\alpha$ -canaphite monoclinic structure, including the hydrogen bonding network. Synchrotron X-ray diffraction and neutron diffraction are combined with multinuclear solid state NMR experimental data and computational modeling via DFT/GIPAW calculations. Among the main characteristics of the  $\alpha$ -canaphite structure are some strong hydrogen bonds and one of the four water molecules showing a different coordination scheme. This peculiar water molecule could be the last to leave the collapsed structure on heating, leading eventually to anhydrous  $\alpha$ - $\text{CaNa}_2\text{P}_2\text{O}_7$  and could also be involved in the internal hydrolysis of pyrophosphate ions as it is the closest water molecule to the pyrophosphate ions. Relating such detailed structural data on  $\alpha$ -canaphite to its physico-chemical properties is of major interest considering the possible roles of canaphite for biomedical applications. The vibrational spectra of  $\alpha$ -canaphite (deuterated or not) are analyzed and Raman spectroscopy appears to be a promising tool for the identification/diagnosis of such microcrystals *in vitro*, *in vivo* or *ex vivo*.

DOI: 10.1039/d0ce00132e

## Introduction

Condensed phosphate structures have received much less attention than the orthophosphate ones. All polyphosphates are indeed hydrolyzed in aqueous solutions, and it has long been considered that this hydrolytic degradation is the cause of the quasi-absence of polyphosphate geological minerals. Pyrophosphates (*i.e.* diphosphates  $\text{P}_2\text{O}_7^{4-}$ ) are the most stable polyphosphate anions, and interestingly, hydrated calcium

pyrophosphate salts are encountered in both geological and biological environments.<sup>1–3</sup> In the field of geological minerals, calcium disodium pyrophosphate tetrahydrate, also called canaphite ( $\text{CaNa}_2\text{P}_2\text{O}_7 \cdot 4\text{H}_2\text{O}$ ), has been identified as the first example of a condensed phosphate geological mineral.<sup>2</sup> The only forms of persistent polyphosphates identified in biological extracellular media are the calcium pyrophosphate dihydrates  $\text{Ca}_2\text{P}_2\text{O}_7 \cdot 2\text{H}_2\text{O}$  (monoclinic and triclinic, m-CPPD and t-CPPD respectively), which occur in the joints of patients suffering from pseudogout.<sup>4,5</sup> Pritzker *et al.*<sup>6</sup> also reported the possible formation of canaphite *in vitro* after 24 h at 10 °C or 37 °C in a crystallization model system involving sodium pyrophosphate and calcium chloride diffusion in cadaveric articular hyaline cartilage (raw or denatured). Moreover, Mandel *et al.*<sup>7</sup> studied m-CPPD and t-CPPD crystal deposition by *in vitro* modeling, and their results revealed the formation of  $\alpha$ - and  $\beta$ -canaphite crystals as minor phases in a biological grade gelatin gel at physiological pH.

Few studies related to canaphite have been published so far. Two polymorphs of canaphite, namely  $\alpha$  and  $\beta$ , have been identified as monoclinic structures and the  $\gamma$  polymorph structure remains unknown.<sup>2,8</sup> Cheng *et al.*<sup>9</sup> obtained the

<sup>a</sup> CIRIMAT, Université de Toulouse, CNRS, Toulouse INP ENSIACET, Toulouse, France. E mail: christele.combes@ensiacet.fr

<sup>b</sup> ICGM, Univ Montpellier, CNRS, ENSCM, Montpellier, France

<sup>c</sup> Sorbonne Université, CNRS, Laboratoire de Chimie de la Matière Condensée de Paris, UMR 7574, Paris, France

<sup>d</sup> Vice Chancellor's Office, Highfield Campus, University of Southampton, University Road, Southampton, SO17 1BJ, UK

<sup>e</sup> Department of Chemistry, Lancaster University, Bailrigg, Lancaster, LA1 4YB, UK

<sup>f</sup> Department of Physics, University of Warwick, CV47AL Coventry, UK

<sup>g</sup> Laboratoire Léon Brillouin, CEA Saclay, Gif sur Yvette, France

<sup>h</sup> Synchrotron Soleil, L'Orme les Merisiers, St. Aubin, Gif sur Yvette, France

† Electronic supplementary information (ESI) available: Tables: S1–S4, figures: S1–S5. CCDC 1989793 and 1989794. For ESI and crystallographic data in CIF or other electronic format see DOI: 10.1039/d0ce00132e

$\beta$ -canaphite phase by diffusion of solutions in hydrogel-like media mimicking the synovial fluids, and they were able to determine its crystal structure. Subsequently, Cheng and Pritzker<sup>8</sup> synthesized the  $\alpha$ -canaphite phase at room temperature by adding a sodium pyrophosphate solution at neutral pH into a calcium salt solution. They showed that this  $\alpha$  phase crystallized in the monoclinic system with the *Pc* space group, but the positions of hydrogen atoms were not determined. Later, Rouse *et al.*<sup>2</sup> confirmed this monoclinic structure and reported its extensive interatomic distance and angle data, making a comparison to the data from Cheng and Pritzker.<sup>8</sup> The hydrogen atom positions were still missing.

Following these initial studies, Cave<sup>10</sup> synthesized  $\alpha$ -canaphite according to a modified protocol from Cheng and Pritzker.<sup>8</sup> This involved pouring together cationic and anionic solutions whereupon precipitation occurred without the need of neutralizing the pyrophosphate solution. The precipitate was then matured overnight. Examination of the XRD pattern presented suggested that an amorphous phase might be present in the as-synthesized  $\alpha$ -canaphite sample. This observation was supported by the estimated number of structural water molecules from thermogravimetric analysis (3.5 per formula unit) as this is not consistent with the stoichiometry of pure  $\alpha$ -canaphite. Another method claimed that  $\alpha$ -canaphite could be prepared by mechanical grinding of a mixture of precursor salts for several hours in the presence of water, leading to a fairly pure phase, containing 5% w/w impurities.<sup>11</sup>  $\alpha$ - and  $\beta$ -canaphite both possess a layered structure which could exhibit specific dehydration and ion exchange properties. The reactivity of canaphite was successfully investigated by reflux reaction of canaphite for two hours in potassium nitrate saturated solution leading to an anhydrous potassium pyrophosphate phase following a structural rearrangement.<sup>10</sup>

A FTIR and Raman vibrational spectroscopic study of synthetic  $\alpha$ -canaphite did not present evidence of sample purity.<sup>12</sup> To the best of our knowledge, no solid state NMR studies of canaphite polymorphs have been reported so far, in contrast to other crystalline calcium pyrophosphate phases, which have been studied by the <sup>1</sup>H, <sup>31</sup>P and <sup>43</sup>Ca magic angle spinning (MAS) solid state NMR techniques.<sup>13–16</sup> A small number of papers concerning canaphite to date have all referred to the synthesis protocol by Cheng and Pritzker,<sup>8</sup> with some adaptations. However, both the protocol and its modifications are poorly described in the literature. In addition, the synthetic canaphite samples were not fully characterized to check for their purity before further structural investigations.

Considering the potential development of canaphite-based biomaterials and/or canaphite identification/diagnosis in the biomedical field, it is essential to thoroughly study its structure. This will allow a better understanding of diseases associated with calcium pyrophosphate-based crystal deposition and the related material properties. In addition, this will allow the potential of such a compound as an

innovative bioactive bone substitute material based on enzyme- and/or pH-driven pyrophosphate ( $P_2O_7^{4-}$ ) hydrolysis into orthophosphate ( $PO_4^{3-}$ ) to be better understood.<sup>17</sup> In this context, the present study initially described a robust protocol for the synthesis of pure  $\alpha$ -canaphite. Then, an advanced multiscale characterization methodology combining synchrotron and laboratory experimental techniques and computational modeling tools is applied to thoroughly characterize the phase from the atomic scale to the macroscopic scale. This provides a full solution of the crystal structure, including the positions of hydrogen atoms.

## Materials and methods

### Precursors

Calcium chloride dihydrate salt ( $CaCl_2 \cdot 2H_2O$ , 100.2%, VWR Chemicals) was used as received. The pyrophosphate precursor, anhydrous tetrasodium pyrophosphate ( $Na_4P_2O_7$ ), was prepared by heating disodium hydrogen phosphate ( $Na_2HPO_4$ , 99%, Merck) at 400 °C for 15 hours in a muffle furnace. The purity of the as-prepared sodium pyrophosphate precursor was checked by XRD, Raman and <sup>31</sup>P solid state NMR spectroscopies (no residual orthophosphate was detected, Fig. S1†) before its use for  $\alpha$ -canaphite synthesis.

### $\alpha$ -Canaphite synthesis

$\alpha$ -Canaphite powder was synthesized by double decomposition in solution (precipitation) at room temperature using an original protocol. Calcium and phosphate reagent solutions were prepared separately by dissolving 2.11 g of  $CaCl_2 \cdot 2H_2O$  (0.0144 moles) in 80 mL of deionized water, and 17.71 g of the as-prepared sodium pyrophosphate ( $Na_4P_2O_7$ ) precursor (0.0666 moles) in 800 mL of deionized water. The calcium solution was then added to the pyrophosphate solution at a constant volumetric flowrate (32 mL min<sup>-1</sup>) using a peristaltic pump. After complete addition, the suspension was left to mature for 24 hours under magnetic stirring, and then filtered and washed with 800 mL of deionized water. The precipitate was finally dried at 37 °C overnight and then stored at 20 °C to prevent any structural evolution before characterization. This synthesis has been performed at least in triplicate to check for its reproducibility.

In view of the fine structural study by neutron diffraction and the FTIR and Raman band assignments, deuterated canaphite was prepared following the protocol detailed above, but with the use of deuterated water ( $D_2O$ , Sigma Aldrich, deuterium oxide 99 atom% D) instead of deionized water to prepare both precursor solutions and washing after filtration. In addition, several precautions were taken at each step of the synthesis protocol to prevent as much as possible any deuterium–hydrogen exchange with water vapor present in the air during powder transfers and storage (hermetically sealed flasks, drying by lyophilization, storage first in a dessicator with a deuterated water saturated atmosphere). Finally, the

sample was vacuum-packed in a plastic bag and stored in a freezer before its analysis.

### **$\alpha$ -Canaphite characterization**

The as-synthesized  $\alpha$ -canaphite powder was fully characterized using complementary multiscale laboratory and synchrotron and neutron techniques for structural, microstructural, molecular and elemental investigations, in combination with computational DFT modeling tools.

**Powder X-ray diffraction (XRD).** A preliminary XRD analysis was performed at room temperature using a laboratory X-ray diffractometer (INEL Symphonix 1000) with a cobalt anticathode ( $\lambda(K_{\alpha}) = 1.788970 \text{ \AA}$ ) and a curved counter to rapidly check the sample purity. Then, the as-synthesized  $\alpha$ -canaphite powder was further analyzed at a synchrotron facility to collect data for structure refinement. Synchrotron powder X-ray diffraction patterns of the synthesized  $\alpha$ -canaphite were acquired at 21 °C on the two-circle diffractometer of the CRISTAL beamline at the SOLEIL synchrotron (Gif-sur-Yvette, France) as part of the project No. 20130932 “*Structural investigations on hydrated calcium pyrophosphate phases of biological interest: study on synthetic and biological samples*”. A monochromatic beam was selected, using a Si (111) double-crystal monochromator, and its wavelength (0.5815 Å) was determined using the NIST standard LaB<sub>6</sub>. The powder sample was placed in a 0.7 mm-diameter special glass capillary mounted on a spinner to improve averaging. High angular resolution was obtained with the 21 perfect Si (111) crystal rear analyzer mounted on the two-circle diffractometer. Detection was performed using Scionix YAP:Ce scintillation detectors.

**Neutron diffraction analysis.** In order to locate precisely the D atoms, neutron powder diffraction (NPD) measurements were performed on the synthesized deuterated  $\alpha$ -canaphite. The experiment was carried out on the G44 diffractometer on the S2 cold source at the Orphée-LLB reactor (France). The diffractogram was recorded at 40 °C using a Ge004 monochromator at a neutron wavelength of 1.959 Å between  $2\theta = 6.00^\circ$  and  $161.30^\circ$  with steps of  $0.05^\circ$ . At  $2\theta$  between  $149.00^\circ$  and  $152.00^\circ$ , the cryofurnace used gave rise to a parasitic peak and this zone had to be excluded from subsequent analyses.

**Structure refinements.** D atoms were located from difference Fourier maps calculated with the NPD data. Subsequent Rietveld refinements were performed using the JANA 2006 software from the joint NPD and synchrotron XRD data. Because this procedure imposed a common value of the cell parameters for the two sets of measurements (synchrotron X-ray and neutron diffraction measurements), both wavelengths were refined in order to account for potential discrepancies in the peak positions; the refined values remained close to the initial values. Distance (H–O distances within 0.001 Å) and angle (H–O–H =  $104.45(1)^\circ$ ) restraints and equivalence between all isotropic thermal displacement parameters were imposed for the refinement of

the water molecules. All the representations of the refined structure presented in this paper were obtained using Vesta.<sup>18</sup>

**FTIR and Raman vibrational spectroscopic analysis.** A Raman Labram HR 800 confocal microscope (Horiba Jobin Yvon) and laser radiation provided by a 532 nm argon diode laser with a power of 14 mW were used. Each spectrum was acquired with an integration time of 60 seconds and three accumulations. FTIR spectra were obtained using a Nicolet IS50 FT-IR spectrophotometer (Thermo Scientific) at a  $4 \text{ cm}^{-1}$  resolution and 64 scan accumulation, by transmission from a KBr pellet.  $\alpha$ -Canaphite and its deuterated analogue were both analyzed by FTIR and Raman spectroscopy.

**Scanning electron microscopy (SEM).** SEM observations were performed on a LEO 435 VP microscope. Samples were stuck onto double-faced carbon tape and silver sputter-coated before observation.

**Thermal analyses.** Thermogravimetric analysis (TGA) and differential thermal analysis (DTA) were performed in triplicate using a Setaram instrument (Setsys Evolution System) from 20 °C to 1000 °C with a step of 30 min at 1000 °C and a heating rate of 4 °C per minute in an air flow.

**Inductively coupled plasma-optical emission spectrometry (ICP-OES).** The analyses were performed on an ICP Ultima Expert machine (argon flow:  $15 \text{ L min}^{-1}$ ) to determine the calcium, phosphorus and sodium concentrations in triplicate.

**Ultra-high performance liquid chromatography (UHPLC).** A Waters Acquity apparatus coupled with an evaporative light scattering detector (ELSD) was used for the detection and titration of traces of chloride ions. Measurements were done in triplicate.

**Solid state NMR.** The experiments were performed on the non-deuterated  $\alpha$ -canaphite samples to analyze the local environments of <sup>23</sup>Na, <sup>31</sup>P, <sup>43</sup>Ca and <sup>1</sup>H nuclei. All solid state NMR spectra were recorded at 14.1 T on a VNMR-600 MHz spectrometer, except for the <sup>1</sup>H NMR experiments, which were recorded at 20.0 T on a Bruker 850 MHz NMR spectrometer (NEO 4 console). A <sup>1</sup>H spin-echo NMR spectrum was acquired using a 1.3 mm HXY MAS probe tuned to <sup>1</sup>H ( $\nu_0 = 850.23 \text{ MHz}$ ). The experiment was performed at 40 kHz MAS. The spectra were recorded using  $2.1 \mu\text{s } 90^\circ$  and  $4.2 \mu\text{s } 180^\circ$  <sup>1</sup>H pulses, with a 1 rotor period echo delay, and using a 2 s recycle delay. A total of 16 scans were collected. The experiments were performed with the temperature control unit set to 10 °C. The <sup>1</sup>H chemical shifts were referenced to the methyl groups in alanine ( $\delta_{\text{iso}}(^1\text{H}) = 1.20 \text{ ppm}$ ). A <sup>31</sup>P single pulse experiment was performed using a 3.2 mm HXY MAS probe tuned to <sup>1</sup>H ( $\nu_0 = 599.82 \text{ MHz}$ ) and <sup>31</sup>P ( $\nu_0 = 242.81 \text{ MHz}$ ) and spinning at 18 kHz. A  $3 \mu\text{s } 90^\circ$  excitation pulse was used (RF  $\approx 83 \text{ kHz}$ ), with SPINAL-64 <sup>1</sup>H decoupling (RF = 100 kHz) during acquisition. A recycle delay of 800 s was used for full relaxation, and 24 scans were collected. The <sup>31</sup>P chemical shifts were referenced to the phosphate groups in synthetic hydroxyapatite, Ca<sub>10</sub>(PO<sub>4</sub>)<sub>6</sub>(OH)<sub>2</sub> ( $\delta_{\text{iso}}(^{31}\text{P}) = 2.8 \text{ ppm}$ ). A <sup>23</sup>Na single pulse MAS NMR spectrum was recorded using a 3.2 mm HXY MAS probe spinning at 20 kHz, with the

**Table 1** Chemical composition (Ca, P and Na amounts in mmoles per 100 mg of sample and Ca/P and Ca/Na atomic ratios) of the synthesized  $\alpha$  canaphite powder determined by ICP OES compared with the expected values for pure canaphite

	Ca mmoles per 100 mg	P mmoles per 100 mg	Na mmoles per 100 mg	Ca/P	Ca/Na
Synthesized $\alpha$ canaphite	$0.298 \pm 0.002$	$0.587 \pm 0.004$	$0.592 \pm 0.001$	$0.508 \pm 0.006$	$0.503 \pm 0.003$
Theoretical composition	0.301	0.602	0.602	0.5	0.5

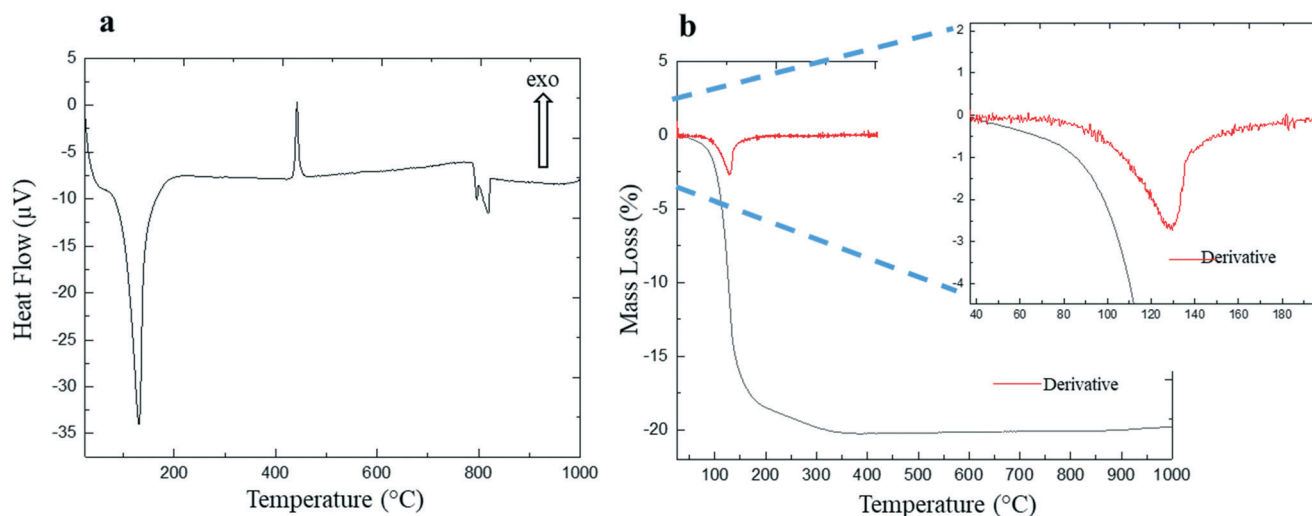


**Fig. 1** DTA (a) and TGA (b) curves of the synthesized  $\alpha$  canaphite powder.

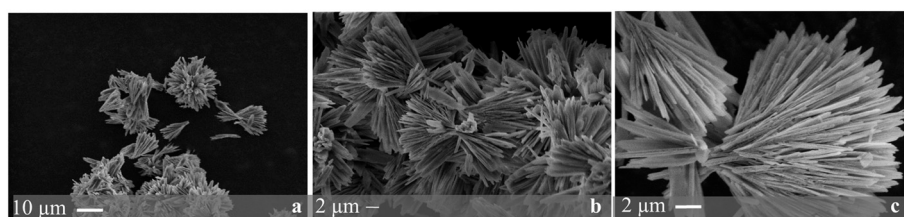


**Fig. 2** SEM micrographs of the synthesized  $\alpha$  canaphite crystals observed at different magnifications.

temperature control unit set to 0 °C. The experiment was performed using a  $0.5 \mu\text{s}$   $30^\circ$   $^{23}\text{Na}$  solid pulse (RF  $\approx$  83 kHz) and spinal-64  $^1\text{H}$  decoupling (RF  $\approx$  100 kHz) during acquisition. A 1 s recycle delay was used, and 6000 scans were collected. The  $^{23}\text{Na}$  NMR chemical shifts were referenced to a 1.0 M NaCl aqueous solution ( $\delta_{\text{iso}}(^{23}\text{Na}) = 0$  ppm). A  $^{43}\text{Ca}$  MAS NMR spectrum was recorded using a 9.5 mm probe, spinning at 4 kHz. A  $3 \mu\text{s}$   $^{43}\text{Ca}$  excitation pulse was used ( $30^\circ$  solid pulse, RF  $\approx$  15 kHz), preceded by a DFS pulse of 4 ms, with a DFS sweep from 250 kHz to 60 kHz in order to increase sensitivity. The spectrum was recorded using a 5 s recycle delay and 31700 scans were co-added. The chemical shifts were referenced to a 1 M  $\text{CaCl}_2$  aqueous solution ( $\delta_{\text{iso}}(^{43}\text{Ca}) = 0$  ppm), while the powers were calibrated on a saturated  $\text{CaCl}_2$  solution. No temperature control was applied.

**Computational studies.** The unit cell parameters were set to the combined neutron/synchrotron X-ray diffraction data and kept fixed during geometry optimizations to ensure

consistency between the experimental and optimized structures. Atomic positions were then relaxed with the VASP (Vienna *ab initio* simulation package) code<sup>19</sup> based on the Kohn–Sham density functional theory (DFT) and using the *a* plane-wave pseudopotential approach. Two situations were tested: relaxing H positions only or all atomic positions. The NMR parameters were then calculated within Kohn–Sham DFT using the QUANTUM-ESPRESSO code,<sup>20,21</sup> keeping the atomic positions equal to the values previously calculated with the VASP. The PBE generalized gradient approximation<sup>22</sup> was used and the valence electrons were described by norm conserving pseudopotentials<sup>23</sup> in the Kleinman–Bylander form.<sup>24</sup> The shielding tensor was computed using the gauge including projector augmented wave (GIPAW) approach,<sup>25</sup> which enables the reproduction of the results of a fully converged all electron calculation.<sup>26</sup> The isotropic chemical shift  $\delta_{\text{iso}}$  is defined as  $\delta_{\text{iso}} = [\sigma - \sigma_{\text{ref}}]$  where  $\sigma$  is the isotropic shielding and  $\sigma_{\text{ref}}$  is the isotropic shielding of the same



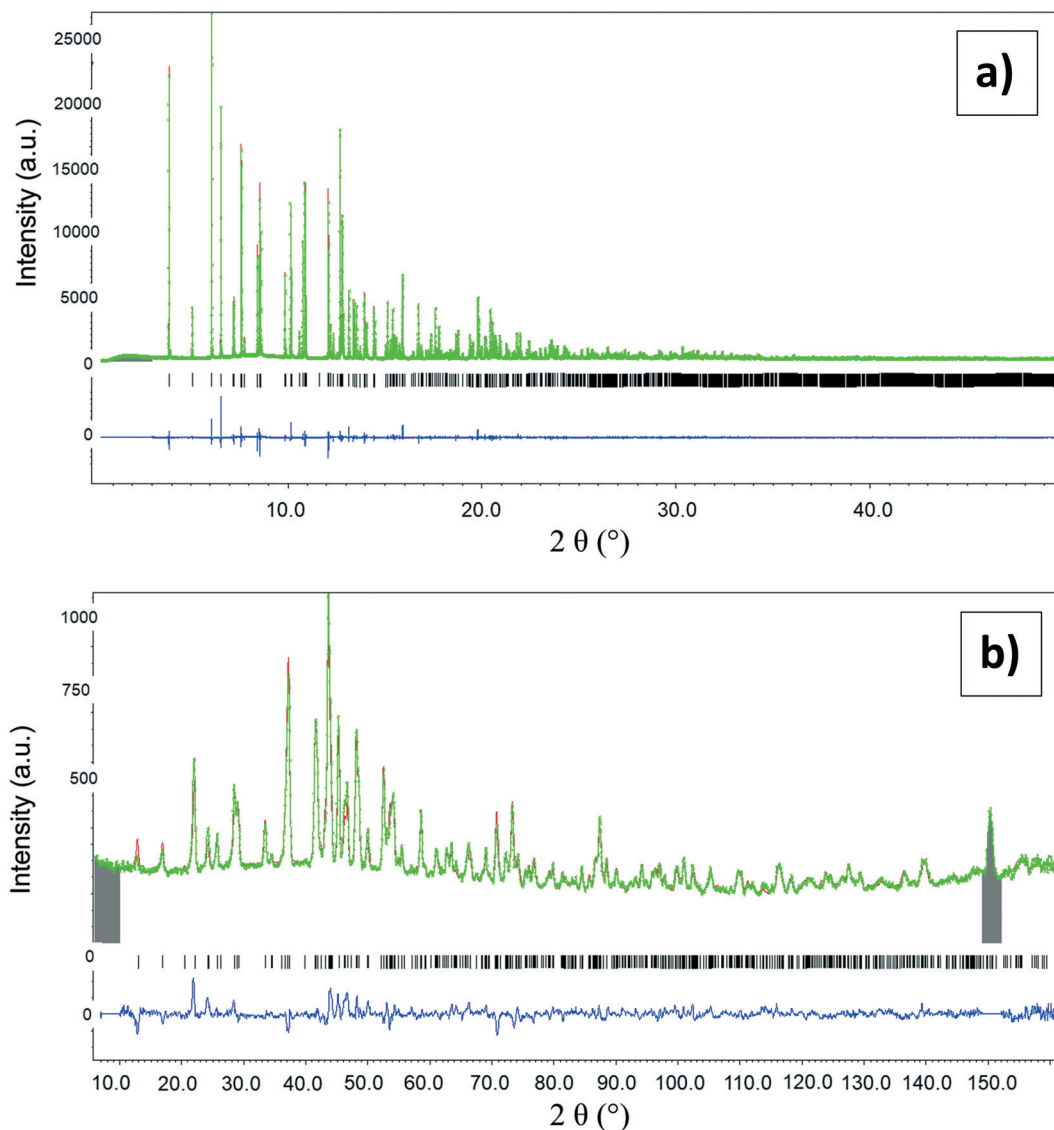


**Fig. 3** Rietveld refinement plots from the powder synchrotron X ray diffraction data (a) and neutron diffraction data (b) of the synthesized  $\alpha$  canaphite (non deuterated (a) and deuterated (b)). Experimental and simulated diagrams and difference are shown; vertical lines indicate the Bragg peak positions (the grey zone around  $150^\circ$  on the neutron diffraction pattern (b) corresponds to a parasitic peak related to the cryofurnace, which is excluded in data refinement).

nucleus in a reference system.  $\sigma_{\text{ref}}$  was fixed so that the average sums of the experimental and calculated shifts of a series of reference compounds coincide, typically calcium phosphates and pyrophosphates for  $^{31}\text{P}$  and  $^{43}\text{Ca}$ ,<sup>27</sup> and sodium phosphates and silicates for  $^{23}\text{Na}$ . The principal components  $V_{xx}$ ,  $V_{yy}$ , and  $V_{zz}$  of the electric field gradient (EFG) tensor defined as  $|V_{zz}| \geq |V_{xx}| \geq |V_{yy}|$  are obtained by diagonalization of the calculated tensor. The quadrupolar interaction can then be characterized by the quadrupolar coupling constant  $C_Q$  and the asymmetry parameter  $\eta_Q$ , which are defined as:  $C_Q = eQV_{zz}/h$  and  $\eta_Q = (V_{yy} - V_{xx})/V_{zz}$  ( $e$  is the proton charge,  $h$  is Planck's constant and  $Q$  the quadrupole moment of the considered nucleus).  $Q$  values of 104 and 44.4 mb were used for  $^{23}\text{Na}$  and  $^{43}\text{Ca}$ , respectively, in agreement with the values reported by Pyykkö and Bryce.<sup>28,29</sup>

## Results and discussion

### Composition of the synthesized powder

Preliminary X-ray diffraction laboratory analysis of the as synthesized canaphite powders showed that these samples correspond to the  $\alpha$ -canaphite phase according to the ICSD data (no. 26015) (Fig. S2†). The elemental composition (Ca, Na and P) of the powder was determined by ICP-OES (Table 1). The experimental values were in agreement with the theoretical ones. In addition, attempts to detect chloride ions (counter ions from the calcium salt precursor, *i.e.*  $\text{CaCl}_2 \cdot 2\text{H}_2\text{O}$ ) using UHPLC were unsuccessful (below the detection limit, *i.e.*  $<1.00 \times 10^{-6}$  mol of Cl in 100 mg of sample). Such thorough elemental characterization, which was not performed in previously published studies, is essential to

**Table 2** Experimental and structure refinement details of the synchrotron X ray and neutron diffraction data

	Synchrotron XRD	Neutron diffraction
Crystal data		
Chemical formula	CaNa <sub>2</sub> P <sub>2</sub> O <sub>7</sub> ·4H <sub>2</sub> O	CaNa <sub>2</sub> P <sub>2</sub> O <sub>7</sub> ·4D <sub>2</sub> O
$M_r$	680.22 g mol <sup>-1</sup> (deuterated)	
$a; b; c$ (Å)	5.690940(7); 8.58811(1); 10.50960(1)	
$\beta$ (°)	105.09130(10)	
$V$ (Å <sup>3</sup> )	495.936(1)	
$Z$	2	
Crystal system, space group	Monoclinic, $Pn$	
Radiation type	X ray ( $\lambda$ 0.58144 Å)	Neutron ( $\lambda$ 1.9605 Å)
Specimen	White powder	
Data collection		
Diffractometer	Cristal beamline (Soleil synchrotron)	G44 beamline (LLB Orphée reactor)
Specimen mounting	$\emptyset$ 0.7 mm capillary	$\emptyset$ 8 mm V container
$2\theta$ values (°)	$2\theta_{\min}$ 3.002° $2\theta_{\max}$ 49.996° $2\theta_{\text{step}}$ 0.002°	$2\theta_{\min}$ 6.01° $2\theta_{\max}$ 161.19° $2\theta_{\text{step}}$ 0.05°
Temperature	294 K	233 K
Refinement agreement factors		
Rp	0.0597	0.0370
Rwp	0.0774	0.0497
Gof	2.09	0.78
No. of data points	23 498	2962
Overall refinement agreement factors		
Rp	0.0580	
Rwp	0.0765	
Gof	1.98	
Computer programs: Jana2006.		

further study and discuss the related structure and properties of  $\alpha$ -canaphite.

TGA of the synthesized  $\alpha$ -canaphite showed that the mass loss, related to the water release, occurred in two steps between  $\approx 70$  °C and  $\approx 160$  °C (confirmed by the first derivative curve in red, Fig. 1b). The mass loss is stabilized at  $\approx 400$  °C corresponding to the total removal of water. The total mass loss reached  $21.4 \pm 0.5\%$  and allowed the determination of the number of water molecules associated with the as-synthesized  $\alpha$ -canaphite:  $3.92 \pm 0.09$ . This value is close to that expected theoretically. The DTA curve (Fig. 1a) revealed the presence of an exothermic peak at about 440 °C which corresponds to a recrystallization phenomenon. The as-synthesized  $\alpha$ -canaphite powder was treated at 400 °C and 600 °C for 15 h to identify the recrystallization product. The XRD analysis of both heat-treated powders (at 400 °C and 600 °C) revealed the formation of the same anhydrous crystalline phase:  $\alpha$ -CaNa<sub>2</sub>P<sub>2</sub>O<sub>7</sub> (triclinic) which has been already described by Bennazha *et al.*<sup>30</sup> However, a shift of the diffraction peaks leading to slightly different unit cell parameters compared to the data reported in the literature was observed (data not shown). The current refined structural data of the as-prepared  $\alpha$ -CaNa<sub>2</sub>P<sub>2</sub>O<sub>7</sub> are presented in Table S1.† The dehydration of  $\alpha$ -canaphite will be discussed later, after the presentation of its fine structural characterization.

All together, the first results demonstrated that the original protocol developed for  $\alpha$ -canaphite powder synthesis by double decomposition in solution at room temperature is reproducible and confirms the obtainment of the

$\alpha$ -canaphite crystalline phase (CaNa<sub>2</sub>P<sub>2</sub>O<sub>7</sub>·4H<sub>2</sub>O). The lack of any small amount of an amorphous compound with a calcium disodium pyrophosphate tetrahydrate composition in the synthesized sample will be checked later by solid state NMR.

### Morphological characterization of the synthesized $\alpha$ -canaphite crystals

SEM was used to determine the morphology of the  $\alpha$ -canaphite particles (Fig. 2). The particles presented a bundle-like morphology, including platelet-like crystals gathered at the middle of the bundle. The characteristic size of these platelets was approximately 11.0  $\mu\text{m}$  in length, 2.0  $\mu\text{m}$  in width and 0.1  $\mu\text{m}$  in thickness (Fig. 2). The platelet morphology of the individual  $\alpha$ -canaphite crystals could be related to its layered structure. The bundle-like organization of the as-prepared  $\alpha$ -canaphite crystals is similar to that of natural canaphite mineral referenced in a mineralogy database (for example: mindat.org). It can be hypothesized that such bundle-like crystal agglomerates result from a spherulite formation process which generally occurs when the driving force for crystallization (*i.e.* supersaturation) is quite high or when the crystal habit is highly oriented; the platelet-like morphology of  $\alpha$ -canaphite crystals could favor this organization as a polycrystalline growth system.<sup>31</sup> Category 1 spherulites are known to grow radially from the nucleation site whereas category 2 spherulites start to grow like thread fibers leading to a crystal sheaf after branching

**Table 3** Selected geometric parameters of the  $\alpha$  canaphite structure (Å, °). P O, Ca O and Na O bond lengths (Å) (P1, P2, Ca1, Na1, Na2). Exp.: data obtained from the refinement of both neutron/synchrotron X ray diffraction data. Tot. rel.: data obtained after DFT relaxation of all positions, starting from the Exp. positions (see Materials & methods). O P O angles (°) and hydrogen bond lengths (Å) and angles (°) are given as well

P1 tetrahedron			P2 tetrahedron					
	Exp.	Tot. rel.		Exp.	Tot. rel.			
P1 O2	1.508(4)	1.5324	P2 O1	1.523(4)	1.5299			
P1 O5	1.542(3)	1.5424	P2 O3	1.536(4)	1.5399			
P1 O7	1.536(4)	1.5232	P2 O6	1.517(3)	1.5247			
P1 O11	1.620(4)	1.6278	P2 O11	1.631(4)	1.6572			
Ca1 octahedron			Na1 octahedron			Na2 octahedron		
	Exp.	Tot. rel.		Exp.	Tot. rel.		Exp.	Tot. rel.
Ca1 O2	2.349(3)	2.3397	Na1 O1	2.448(5)	2.4470	Na2 O1	2.407(4)	2.3990
Ca1 O3	2.347(4)	2.3618	Na1 Ow4	2.347(4)	2.3290	Na2 O2	2.393(4)	2.4239
Ca1 O5	2.357(4)	2.3814	Na1 O6	2.435(4)	2.4499	Na2 O3	2.755(4)	2.7654
Ca1 O6	2.326(4)	2.3321	Na1 Ow8	2.416(4)	2.3940	Na2 Ow4	2.336(5)	2.3430
Ca1 O7	2.285(4)	2.3009	Na1 Ow9	2.421(5)	2.4224	Na2 Ow9	2.395(4)	2.3710
Ca1 Ow8	2.387(4)	2.4376	Na1 Ow10	2.749(5)	2.6750	Na2 Ow10	2.377(5)	2.4114
P1 tetrahedron			P2 tetrahedron			P1 O11 P2		
	Exp.	Tot. rel.		Exp.	Tot. rel.		Exp.	Tot. rel.
O2 P1 O5	111.2(2)	111.1	O1 P2 O3	111.0(2)	112.6		129.9(3)	129.8
O2 P1 O7	112.7(2)	113.3	O1 P2 O6	115.7(2)	115.2			
O2 P1 O11	108.53(2)	108.1	O1 P2 O11	103.6(2)	101.5			
O5 P1 O7	111.24(2)	112.0	O3 P2 O6	112.7(2)	112.4			
O5 P1 O11	108.53(2)	107.9	O3 P2 O11	106.9(2)	106.8			
O7 P1 O11	104.3(2)	103.8	O6 P2 O11	106.0(2)	107.2			
	D H		H...A		D A		D H...A (°)	
D H...A	Exp.	Tot. rel.	Exp.	Tot. rel.	Exp.	Tot. rel.	Exp.	Tot. rel.
Ow4 H2...Ow10	0.83(1)	0.977	2.20(2)	2.020	2.945(5)	2.912	150(2)	150.8
Ow4 H3...O7	0.83(3)	0.994	1.86(2)	1.699	2.659(5)	2.686	162(3)	171.3
Ow8 H5...O5	0.83(2)	0.999	1.96(1)	1.717	2.772(5)	2.712	167(3)	172.8
Ow9 H6...O5	0.83(2)	0.982	2.11(2)	1.905	2.924(5)	2.882	166(3)	172.5
Ow10 H8...O3	0.83(2)	0.996	2.05(3)	1.802	2.861(6)	2.786	167(3)	168.9
Ow9 H11...O1	0.83(2)	0.991	1.91(2)	1.767	2.737(5)	2.750	175(3)	170.7
Ow8 H13...O2	0.83(2)	0.984	2.25(2)	2.022	3.000(5)	2.969	151(3)	160.9

which finally ends as a sphere after longer evolution times. The organization of  $\alpha$ -canaphite platelet crystals observed by SEM (Fig. 2) corresponds to a category 2 spherulite growth (Fig. 2b and c). However, it appears that some of the observed category 2 spherulites are not perfectly symmetric and some of the platelet crystals are disassembled and/or fragmented (Fig. 2a); the 24 h-maturation under magnetic stirring, filtration, and washing are the steps for canaphite synthesis that could have altered the growth of these spherulites. The formation of category 2 spherulites was also identified for monoclinic calcium pyrophosphate tetrahydrate (m-CPPT  $\beta$ ) and dihydrate (m-CPPD) crystal formation from amorphous calcium pyrophosphate evolution in solution at pH = 5.8 and 50 °C.<sup>32</sup>

### Fine structural characterization of the as-synthesized $\alpha$ -canaphite phase

The as-synthesized non-deuterated and deuterated  $\alpha$ -canaphite samples were analyzed by synchrotron X-ray diffraction and neutron diffraction, respectively (Fig. 3).

Then, Rietveld refinements were performed from the joint neutron and synchrotron-X-ray diffraction data (Table 2).

The solved  $\alpha$ -canaphite structure presents molecular groups that correspond to pyrophosphate ions and four water molecules, as expected. The asymmetric unit has a composition corresponding to the formula  $\text{CaNa}_2\text{P}_2\text{O}_7 \cdot 4\text{H}_2\text{O}$ , each atom occupying a 2a Wyckoff position of the  $Pn$  space group. The pyrophosphate molecule is thus non-centrosymmetric. Selected bond lengths and angles are reported in Table 3. The structure of the  $\alpha$ -canaphite is composed of alternating pyrophosphate and water layers (oriented along the plane (001)) separated by layers of calcium and sodium cations (Fig. 4). Hydrogen bonds ensure the cohesion of molecules within the layers (Fig. 5).

The P-O-P angle of the pyrophosphate group has often been discussed as an adaptive parameter in a number of structures. Its value can be determined from structural data (129.9(3)° and 129.8° as determined from both neutron/synchrotron X-ray diffraction data refinement and DFT calculations, respectively, Table 3) or from vibrational spectroscopic data as reported by Rulmont *et al.*<sup>33</sup> and other



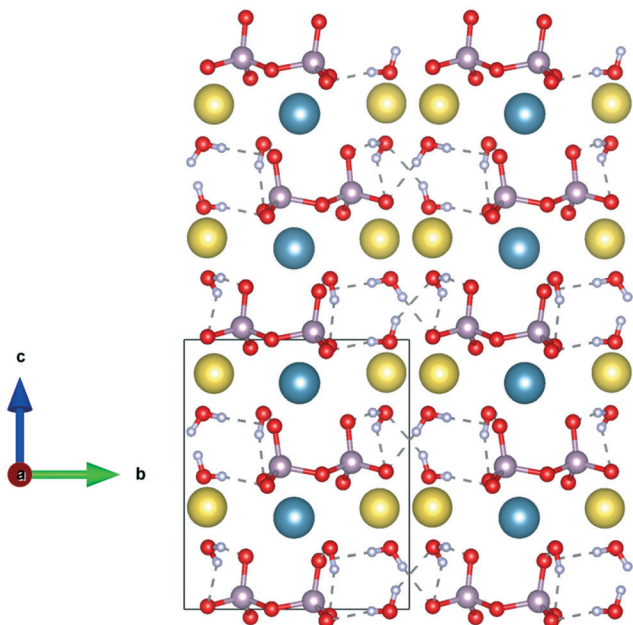


Fig. 4 Three dimensional representation of the monoclinic elemental cell of  $\alpha$ -canaphite, with placement of hydrogen atoms (obtained from refinement of both X ray and neutron diffraction data; yellow: sodium, blue: calcium, grey: phosphorus, red: oxygen, white: hydrogen).

workers<sup>34</sup> with an empirical equation based on the relative position of the symmetric and antisymmetric stretching vibrations of the POP group. Such a determination for  $\alpha$ -canaphite,  $129^\circ$ ,<sup>12</sup> is in agreement with that obtained from the crystal structure. Torsions between the terminal groups are low, linking the canaphite structure to dichromate-type structures which are a common type of structure for hydrated calcium pyrophosphate compounds like triclinic calcium

pyrophosphate dihydrate (t-CPPD), monoclinic calcium pyrophosphate tetrahydrate (m-CPPT  $\beta$ ), anhydrous calcium pyrophosphate and also the anhydrous calcium disodium pyrophosphate  $\alpha$  phase ( $\alpha$ - $\text{CaNa}_2\text{P}_2\text{O}_7$ ).<sup>30,35,36</sup>

Both calcium and sodium atoms are 6-fold coordinated. Calcium is mainly bound to pyrophosphate ions, with only one link to a water ligand through the “OW8” atom. On the contrary, Na1 and Na2 have 4 and 3 coordination bonds with water molecules, respectively. Polyhedra are linked together by one side. Sodium polyhedra are linked to each other and also to calcium polyhedra. Calcium polyhedra, on the other hand, are linked only to sodium polyhedra. These units are spaced from each other by pyrophosphate molecules (Fig. 6). The cationic chains thus formed are staged, linking Na1–Ca1–Na2 blocks oriented along the  $[120]$  and  $[\bar{1}20]$  axes. We can also note the different coordinations of the Ow4, Ow9 and Ow10 atoms, only with sodium ions, and Ow8 with sodium–calcium binding (Fig. 4 to 6).

As mentioned by Cheng *et al.*,<sup>9</sup> the  $\alpha$ - and  $\beta$ -calcium disodium pyrophosphate tetrahydrate structures are very similar, the main differences being the organization of the  $\text{Ca}^{2+} \cdots \text{P}_2\text{O}_7^{4-} \cdots \text{Ca}^{2+}$  chains in relation to the (010) plane. Fig. 7 highlights the close relationship between the two structures, including the organization of the  $\text{CaNa}_2\text{P}_2\text{O}_7 \cdot 4\text{H}_2\text{O}$  units. The most significant differences can be observed on the alternating orientations of pyrophosphate molecules. The intra- and intermolecular distances (Table 3) are significantly similar to those of the  $\beta$ -canaphite structure.<sup>9</sup>

Complementarily, a methodology combining experimental (solid state NMR) and computational methods (first principles GIPAW calculations<sup>25</sup>) was implemented to characterize in detail the structure of  $\alpha$ -canaphite at the atomic level. The  $^{31}\text{P}$ ,  $^1\text{H}$ ,  $^{23}\text{Na}$ , and  $^{43}\text{Ca}$  MAS NMR spectra

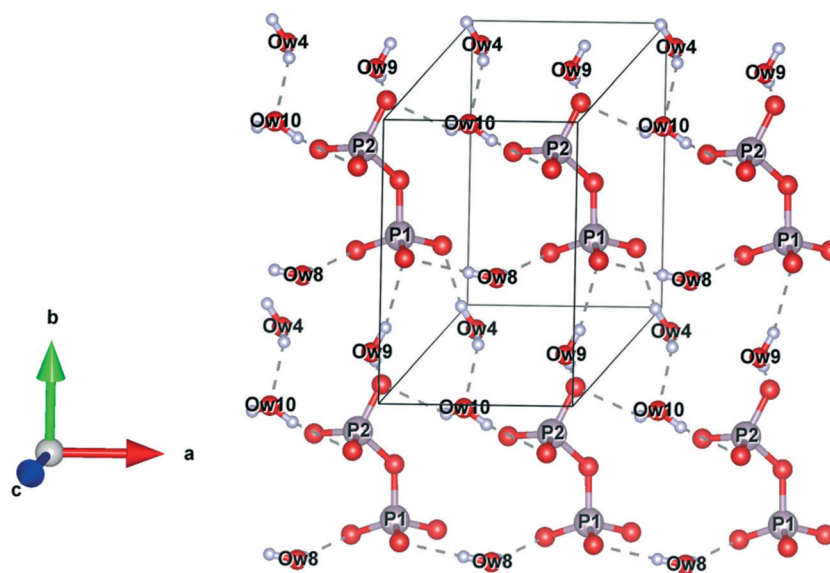


Fig. 5 Representation of hydrogen bonds within the layers of the  $\alpha$ -canaphite. Ow: oxygen atoms of water molecules (grey: phosphorus, red: oxygen, white: hydrogen, sodium and calcium cations are not represented in this figure).

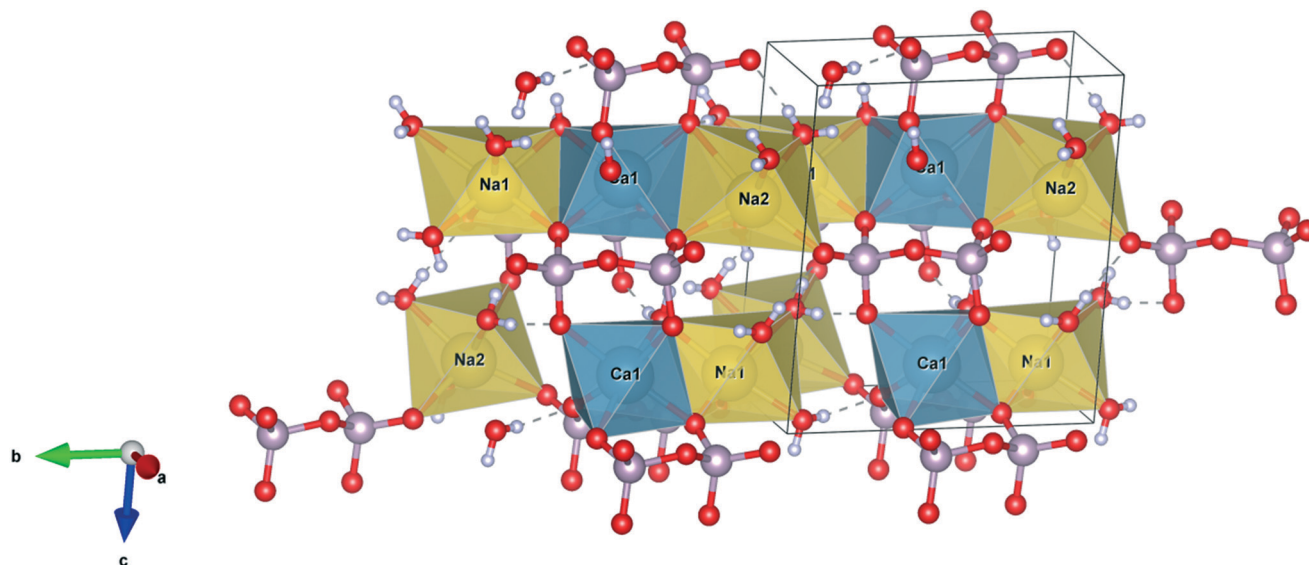


Fig. 6 Representation of calcium and sodium polyhedra of the  $\alpha$ -canaphite structure (yellow: sodium, blue: calcium, grey: phosphorus, red: oxygen, white: hydrogen).

and the corresponding extracted NMR parameters (isotropic chemical shifts, quadrupolar constants,  $C_Q$ , and quadrupolar asymmetries,  $\eta_Q$ ) are given in Fig. 8 and Table 4, respectively.

It should be noted that calculations were performed on the structural models derived from the structure previously presented (Fig. 4 to 6), in which either only H atom positions, or all atomic positions were relaxed by DFT. In the latter case, as discussed below, the agreement with the experimental NMR data is the best. Therefore, the P–O, Ca–O, Na–O and O–H bond lengths obtained after relaxation were added in Table 3. It appears that the P tetrahedra and Ca/Na octahedra geometries are not significantly modified by relaxation. On the other hand, the Ow–H bond lengths originally around 0.83 Å increase up to almost 1 Å after relaxation, a value closer to what is usually expected in water. In parallel, the H $\cdots$ Ow distances decrease after relaxation since the O $\cdots$ O distances are maintained. Moreover, the global architecture of the H-bond network is not modified since the O–H $\cdots$ O angles do not change significantly.

The  $^{31}\text{P}$  MAS NMR spectrum is characterized by two distinct sharp isotropic peaks, in agreement with the presence of one unique pyrophosphate group (P1, P2) in the asymmetric unit. The high signal to noise ratio allows us to conclude safely that potential impurities are completely absent. It follows that  $^{31}\text{P}$  MAS NMR spectroscopy can act as a highly reliable tool of investigation to check the purity of a given  $\alpha$ -canaphite powder sample. The  $^{23}\text{Na}$  MAS spectrum is more complex as  $^{23}\text{Na}$  is a quadrupolar nucleus ( $I = 3/2$ ). Nevertheless, it can be interpreted by the superposition of two contributions (Na1 and Na2, see Table 4) broadened by residual second-order quadrupolar interaction (it is well established that MAS cannot entirely suppress such a kind of second order broadening). Though it is less direct than  $^{31}\text{P}$  MAS NMR analysis,  $^{23}\text{Na}$  MAS NMR remains a complementary method to check the sample purity. The  $^{43}\text{Ca}$  NMR spectrum exhibits a rather featureless

peak corresponding to the unique calcium atom in the asymmetric unit. The broadening of the line is mainly due to the residual second order quadrupolar effect as well, because calcium-43 is a 7/2 spin quadrupolar nucleus. Finally, the  $^1\text{H}$  spin echo MAS NMR spectrum is probably the most difficult to interpret as residual  $^1\text{H}$ – $^1\text{H}$  homonuclear dipolar coupling broadens the line shapes (even spinning at 40 kHz at the magic angle). The shifted  $^1\text{H}$  resonance (above 6 ppm) is in agreement with the presence of some strong H-bonds within the canaphite structure.

GIPAW DFT calculations of the NMR parameters were performed on structural models derived from the neutron/synchrotron X-ray structures, in which either only H atom positions or all atomic positions were relaxed by DFT (Table 4). These calculations were found to be in very good agreement with the experimental data, confirming the accuracy of the final structure of  $\alpha$ -canaphite. In the case of  $^{31}\text{P}$  NMR, the results obtained after total relaxation of the  $\alpha$ -canaphite atomic positions led to improved agreement with the experimental shifts. More importantly, for  $^{31}\text{P}$  and  $^{23}\text{Na}$ , the GIPAW calculations could be used for assigning both sites resolved in NMR spectroscopy. Regarding  $^1\text{H}$  NMR, the overall range of calculated  $^1\text{H}$  chemical shifts was found to be in complete agreement with the corresponding experimental data shown in Fig. 8. Moreover, as previously observed for other pyrophosphate phases, such GIPAW DFT calculations show the strong impact of H-bonding on the  $^1\text{H}$  isotropic chemical shifts.<sup>13</sup> If the positions of the protons are not precise enough, the GIPAW calculations usually diverge.

#### Vibrational spectroscopic analysis of the as-synthesized $\alpha$ -canaphite phase (deuterated and non-deuterated)

$\alpha$ -Canaphite was characterized by FTIR and Raman spectroscopy as well. The vibrational spectrum of crystals can

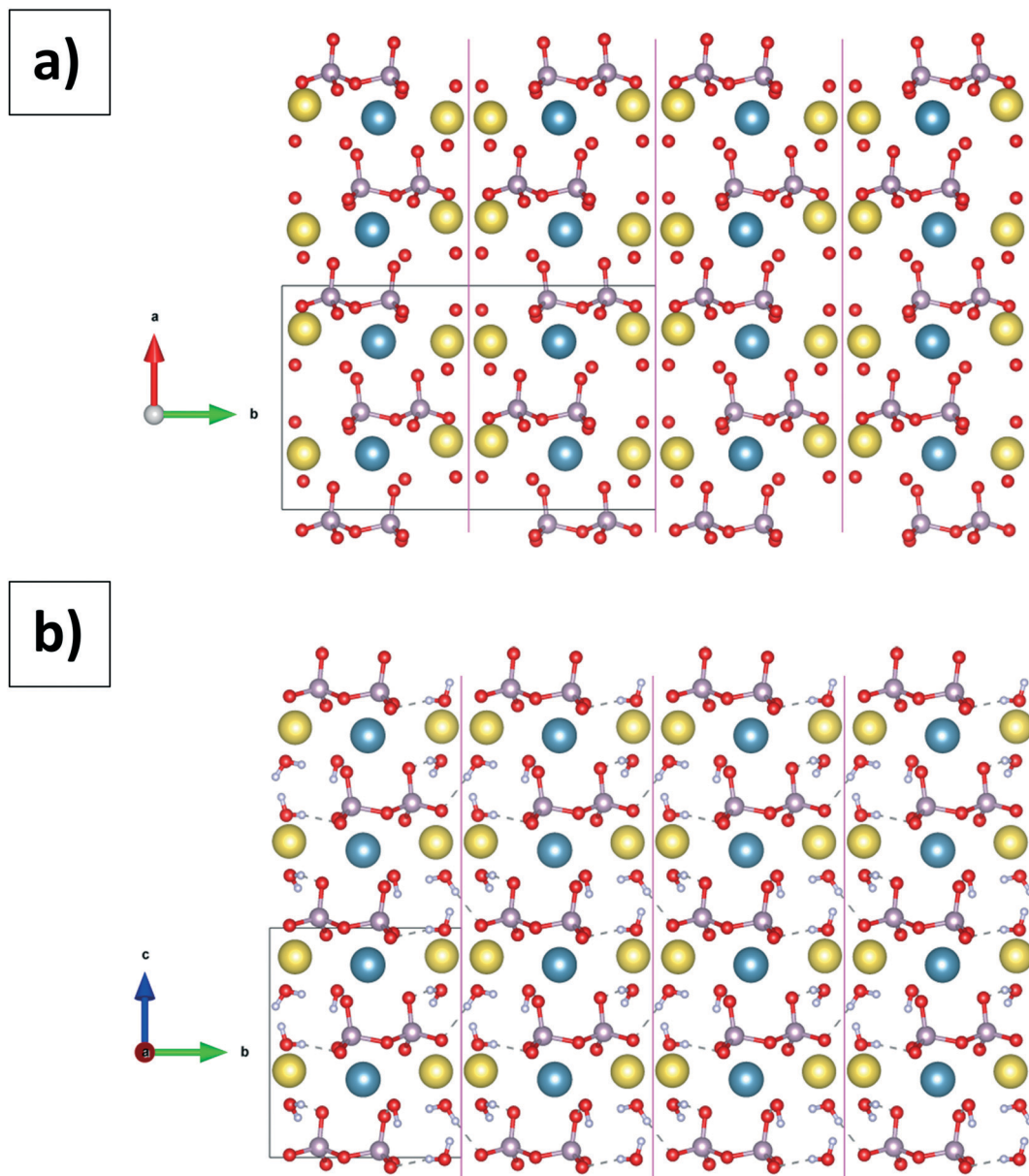


**Fig. 7** Comparison of the  $\beta$  (a)<sup>9</sup> and  $\alpha$  (b) canaphite structures, the (010) planes of interest are shown (yellow: sodium, blue: calcium, grey: phosphorus, red: oxygen, white: hydrogen).

be interpreted using the factor group theory which predicts the number of lines expected and their activity in IR and Raman. Focusing on the internal vibration modes of  $\text{H}_2\text{O}$  ( $\text{D}_2\text{O}$ ) and  $\text{P}_2\text{O}_7^{4-}$  molecular units, respectively, 24 and 42 vibration lines should be expected (see details in the ESI† on vibrational spectroscopies and in Tables S2 and S3†). The Raman full spectrum of the as-synthesized  $\alpha$ -canaphite powder is presented in Fig. S3† and the  $\text{H}_2\text{O}$  ( $\text{D}_2\text{O}$ ) and  $\text{P}_2\text{O}_7^{4-}$  molecular vibrational domains (FTIR and Raman) are presented in Fig. 9. The different FTIR and Raman lines and their respective assignments for  $\alpha$ -canaphite and its deuterated analogue are reported in Table S4.† Obviously, all the 66 lines predicted for the internal vibration modes cannot be distinguished, due to line broadening and superimpositions.

Generally several vibrational domains can be distinguished depending of the vibration energy. For  $\text{P}_2\text{O}_7^{4-}$  stretching vibrations ( $1200\text{--}700\text{ cm}^{-1}$ ), the two  $\text{PO}_3$  groups and the POP bridge are considered and their vibration domain is well identified (Fig. 9a). In the  $1200\text{--}1000\text{ cm}^{-1}$  range, the two  $\text{PO}_3$  groups of each pyrophosphate ion should show different lines (three for each group, distinguished as one symmetric and two antisymmetric vibrations), and the group factor effect could split again these lines. Generally one very strong  $\nu_s$  line is visible on the Raman spectrum of  $\alpha$ -canaphite and many other pyrophosphate salts.<sup>12,37</sup> For the POP bridge, two stretching modes, symmetric and antisymmetric, are found in the free ion ( $950\text{--}700\text{ cm}^{-1}$ ); in  $\alpha$ -canaphite, these could also be split according to factor

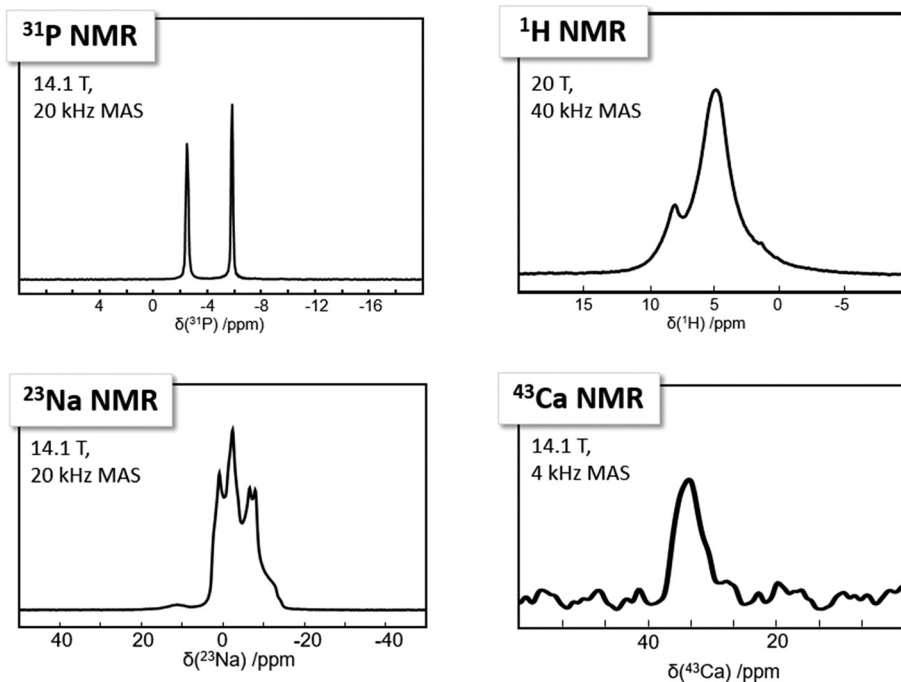


**Fig. 8**  $^{31}\text{P}$ ,  $^{23}\text{Na}$ , and  $^{43}\text{Ca}$  MAS NMR spectra at 14.1 T and  $^1\text{H}$  spin echo MAS NMR spectrum at 20.0 T of the as synthesized  $\alpha$ -canaphite powder. All experimental details are given in the Materials and methods section.

**Table 4**  $^{31}\text{P}$ ,  $^{23}\text{Na}$ ,  $^{43}\text{Ca}$ , and  $^1\text{H}$  experimental and extracted data for the as synthesized  $\alpha$ -canaphite powder. Computational details related to GIPAW calculations<sup>25</sup> are given in the Materials and methods section. Tot. rel. calc.: GIPAW data obtained after DFT relaxation of all positions (see caption of Table 3). Rel. H calc.: GIPAW data obtained after DFT relaxation of H positions only

	Rel. H calc.			Tot. rel. calc.			Experimental		
	$\delta_{\text{iso}}/\text{ppm}$	$C_Q/\text{MHz}$	$\eta_Q$	$\delta_{\text{iso}}/\text{ppm}$	$C_Q/\text{MHz}$	$\eta_Q$	$\delta_{\text{iso}}/\text{ppm}$	$C_Q/\text{MHz}$	$\eta_Q$
P1	-1.8			-5.5			-5.8 (0.1)		
P2	2.6			-1.4			-2.5 (0.1)		
Na1	0.2	-2.4	0.99	0.4	2.5	0.82	-0.3 (0.1)	2.20 (0.05)	0.78 (0.02)
Na2	4.6	2.0	0.44	3.3	2.1	0.50	4.0 (0.1)	2.00 (0.05)	0.30 (0.02)
Ca	48.2	-1.5	0.30	33.9	-1.4	0.45			
H2	3.3			3.7					
H3	7.8			7.6					
H4	2.1			2.3					
H5	7.8			8.5					
H6	4.3			4.8					
H8	6.5			7.3					
H11	7.2			6.5					
H13	5.2			5.1					

group considerations. In the spectra obtained, only one  $\nu_s$  POP line is seen at the same position ( $740\text{--}743\text{ cm}^{-1}$ ) in the Raman and FTIR spectra of the deuterated  $\alpha$ -canaphite. In the FTIR spectrum of the  $\text{H}_2\text{O}$  canaphite, this line seems hindered by the broad water libration line at this position. This line, which is much more intense in Raman than in FTIR, is a specific signature of pyrophosphate ions. A  $\nu_{\text{as}}$  POP line is observed in all samples (FTIR and Raman) at  $906\text{--}909\text{ cm}^{-1}$ . In addition, a stronger line is seen at  $938\text{--}934\text{ cm}^{-1}$  only in FTIR, the attribution of which is not clear. Lower energy vibrations corresponding to bending modes of the  $\text{P}_2\text{O}_7$  group are also present, but they seem more difficult to

assign considering the other contributions, especially those of generally broad water libration lines. For  $\text{H}_2\text{O}$  vibrations, the four water molecules in the formula unit show different environments and should exhibit 4 lines for each  $\nu_s$ ,  $\nu_{\text{as}}$  and  $\delta$  vibration modes of the molecule (Fig. 9b). These lines would also be split in virtue of group factor considerations. The Raman and FTIR lines (Fig. 9) are in close positions according to the group theory treatment predicting identical irreducible representations, vibrational energy levels and transitions, for both techniques. This observation confirms the absence of an inversion centre in the  $\text{P}_2\text{O}_7^{4-}$  groups as already noted from the structural data.



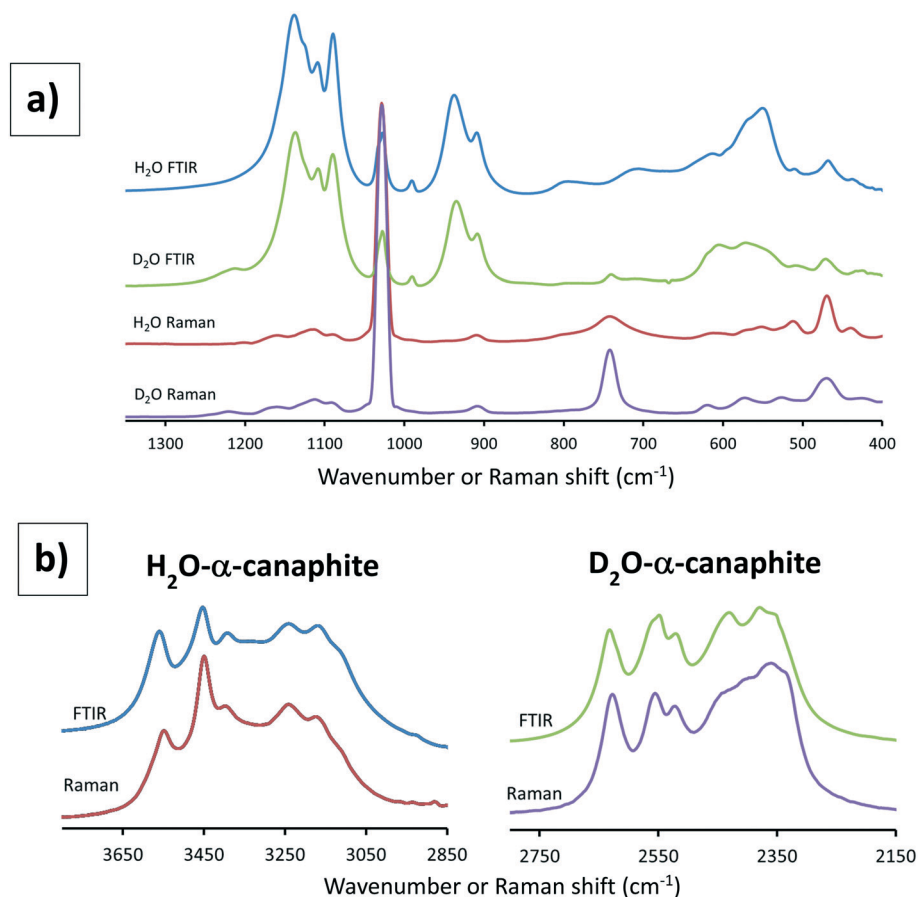


**Fig. 9** FTIR and Raman spectra of the synthesized  $\alpha$  canaphite (deuterated and non deuterated) showing the domains where appear the  $P_2O_7^{4-}$  stretching and bending lines and the  $H_2O$  and  $D_2O$  bending and libration lines (a) and the O H (or O D) water stretching vibrations (b).

The deuteration allows us to distinguish water bands from pyrophosphate ones especially in the bending domains where water libration lines can be easily shifted towards lower wavenumbers (Fig. 9). In particular, such  $H_2O$  lines can be identified at about 800, 706, and 548  $cm^{-1}$ . The faint line at 791  $cm^{-1}$ , in the deuterated sample FTIR spectrum, is attributed to incomplete deuteration of the samples (about 20% residual  $H_2O$ ), possibly due to exchange with air during sample preparation and analysis. Deuteration shifts the water lines to the low energy region (590, 520 and 410  $cm^{-1}$ ) overlapping the  $P_2O_7^{4-}$  ones especially in FTIR. The shift ratio between the  $H_2O$  and  $D_2O$  stretching lines, about 1.35, is in agreement with the theoretical and experimental determinations.<sup>38</sup> The FTIR and Raman determination of the POP angle using Harcharras' diagram<sup>37</sup> based on Lazarev's observations is close to 129°, in agreement with the value obtained from the diffraction data.

#### Further analyses upon heat-treatment

We showed by thermogravimetric analysis that  $\alpha$ -canaphite recrystallized at about 440 °C into the anhydrous calcium disodium pyrophosphate triclinic phase ( $\alpha$ - $CaNa_2P_2O_7$ ). The latter phase is not a layered structure (Fig. S4†) and the

orientation of the pyrophosphate molecules are very different from that in the  $\alpha$ -canaphite structure in which strong hydrogen bonds are also involved as demonstrated by the present fine structural analysis by the diffraction methods, solid state NMR and DFT calculations. These observations suggest that this transformation (crystallization) is probably complex with strong structural reorganization. In addition, the observed dehydration mechanisms could be related to the different coordinations of the Ow4, Ow9 and Ow10 atoms, only with sodium ions, and Ow8 with sodium-calcium binding (Fig. 4 to 6). Indeed, the latter related water molecule (involving Ow8) could be the last one to leave the structure due to the two cation  $Na^+/Ca^{2+}$  binding. This hypothesis is supported by the fact that one water molecule was also differentiated in another hydrated calcium pyrophosphate layered compound, monoclinic calcium pyrophosphate tetrahydrate beta (m-CPPT  $\beta$ ), and identified as the last one to leave the structure upon heating and also the one involved in pyrophosphate internal hydrolysis into orthophosphate.<sup>34</sup> In the case of the  $\alpha$ -canaphite structure, we can hypothesize that the Ow8-related water molecule which is also the one closer to pyrophosphate (distance Ow8-O11 = 3.123 Å) could be the one involved in the internal hydrolysis of pyrophosphate ions. Fig. S5† shows the Raman



spectrum of  $\alpha$ -canaphite dried at 250 °C, an intermediary temperature, *i.e.* higher than 37 °C but lower than that leading to  $\alpha$ -canaphite full dehydration (440 °C). We can observe the appearance of a new band of low intensity at 950  $\text{cm}^{-1}$  characteristic of  $\nu_s \text{PO}_4$ , supporting the hypothesis of the formation of orthophosphate *via* pyrophosphate internal hydrolysis. Currently, we are thoroughly investigating the effect of temperature on the  $\alpha$ -canaphite phase and especially its transformation up to the dehydrated phase ( $\alpha\text{-CaNa}_2\text{P}_2\text{O}_7$ ) involving among others the hydrolysis of pyrophosphate ions upon moderate heating. This hydrolysis leads to the formation of orthophosphate ions which could stabilize a potential intermediary amorphous phase formation; this study will be published in a forthcoming manuscript.

## Conclusion

Canaphite is a layered phosphate of biological interest from the perspective of *in vivo* calcium pyrophosphate-based crystal-associated diseases or as an innovative bone substitute material based on enzyme- and/or pH-driven pyrophosphate ( $\text{P}_2\text{O}_7^{4-}$ ) hydrolysis into orthophosphate ( $\text{PO}_4^{3-}$ ). The novel synthesis protocol developed here is simple, reproducible and enables pure  $\alpha$ -canaphite,  $\text{CaNa}_2\text{P}_2\text{O}_7 \cdot 4\text{H}_2\text{O}$ , to be obtained. Various observations of the phase development are presented. Most importantly, for the first time, the monoclinic crystal structure of  $\alpha$ -canaphite was fully solved (including the positions of hydrogen atoms) by a combination of synchrotron X-ray and neutron diffraction, solid state NMR and DFT calculations. This detailed structural analysis identifies the presence of some strong H-bonds within the  $\alpha$ -canaphite structure. One of the four oxygen atoms from water molecules has a different coordination, *i.e.* the two-cation binding of Ow8 to  $\text{Na}^+$  and  $\text{Ca}^{2+}$ . It is therefore probable that this water is the last one to leave the structure during canaphite dehydration. In addition, the Ow8-related water molecule is much more likely to be involved in the internal hydrolysis of pyrophosphate ions as it is the closest to a pyrophosphate molecule. A thorough study of the  $\alpha$ -canaphite dehydration process is now necessary which will be fully described in a forthcoming paper. The very high signal-to-noise ratios observed from  $^{31}\text{P}$  and  $^{23}\text{Na}$  MAS NMR spectroscopies are suitable to confirm the purity of any sodium pyrophosphate precursor and  $\alpha$ -canaphite.  $^{31}\text{P}$  MAS NMR provides much sharper spectral lines such that both P atoms of the unique pyrophosphate group in the asymmetric unit are completely resolved. The first principles GIPAW calculations provide unambiguous assignments for both  $^{31}\text{P}$  and  $^{23}\text{Na}$  resonance peaks and an interpretation for the dispersion of the  $^1\text{H}$  isotropic chemical shifts related to the H-bond network in the  $\alpha$ -canaphite structure. Finally, vibrational spectroscopies, especially Raman, are a promising tool for fast *in vitro*, *in vivo* or *ex vivo* calcium disodium pyrophosphate microcrystal identification/diagnosis needing only a small amount of the sample. This study provides a full description of the  $\alpha$ -canaphite phase and some initial thermal

property determination. Both are essential to fully exploit the structural and physico-chemical properties of  $\alpha$ -canaphite in materials science, especially for biomedical applications.

## Author contributions

LM and MD carried out the synthesis and routine characterization of the canaphite samples, NJ and MS the NMR experiments, CG the DFT calculations, FP the neutron diffraction analysis and the refinement of diffraction data, EE the synchrotron XRD analysis, PG the preliminary refinement of the diffraction data, CCH the laboratory XRD and TGA-DTA, and CR the vibrational spectroscopy analysis. DL and CB coordinated the NMR and DFT studies and secured funding. JS coordinated the canaphite characterization and supervised LM and MD (PhD students). CCO was the scientific coordinator of the study and of the paper, supervised LM and MD (PhD students) and secured funding. All authors read, participated to correct and approved the final manuscript.

## Conflicts of interest

There are no conflicts to declare.

## Acknowledgements

The authors would like to thank the Agence Nationale de la Recherche (PyVerres project – grant no. ANR-16-CE19-0013) for supporting this research work and the Laboratoire Léon Brillouin and Synchrotron Soleil for the provision of beamtimes (proposals no. 745 and no. 20130932, respectively). The 850 MHz solid-state NMR facility used in this research was funded by the EPSRC and BBSRC, as well as the University of Warwick *via* part funding through the Birmingham Science City Advanced Materials Projects 1 and 2 supported by the Advantage West Midlands (AWM) and the European Regional Development Fund (ERDF). NMR spectroscopic calculations were performed using HPC resources from GENCI-IDRIS (Grant 097535).

## References

- 1 D. R. Peacor, P. J. Dunn, W. B. Simmons and F. J. Wicks, *Mineral. Rec.*, 1985, **16**, 467–468.
- 2 R. C. Rouse, D. R. Peacor and R. L. Freed, *Am. Mineral.*, 1988, **73**, 168–171.
- 3 K. P. Pritzker, in *Calcium phosphates in Biological and Industrial Systems*, ed. Z. Amjad, Kluwer Academic Publishers, 1998, pp. 277–301.
- 4 N. Khon, R. E. Hughes, D. J. McCarty and J. S. Faires, *Ann. Intern. Med.*, 1962, **56**, 738–745.
- 5 P. Richette, T. Bardin and M. Doherty, *Rheumatology*, 2009, **48**, 711–715.
- 6 K. P. Pritzker, P. T. Cheng, S. A. Omar and S. C. Nyburg, *J. Rheumatol.*, 1981, **8**, 451–455.

- 7 N. S. Mandel, G. S. Mandel, D. J. Carroll and P. B. Halverson, *Arthritis Rheum.*, 1984, **27**, 789–796.
- 8 P. T. Cheng and K. P. H. Pritzker, *Acta Crystallogr., Sect. B: Struct. Sci.*, 1980, **36**, 921–924.
- 9 P. T. Cheng, S. C. Nyburg, M. E. Adams and K. P. H. Pritzker, *Cryst. Struct. Commun.*, 1979, **8**, 313–317.
- 10 M. R. Cave, Investigation of layered calcium phosphates and related materials for biomaterial applications, *PhD thesis*, University of Birmingham, United Kingdom, 2010.
- 11 T. V. Safronova, V. I. Putljaev, P. A. Sechejko and J. D. Tret'jakov, *Russian Pat.*, RU2499767C1, 2012.
- 12 I. Hubert Joe, G. Aruldas and G. Keresztury, *J. Raman Spectrosc.*, 1991, **22**, 537–539.
- 13 P. Gras, A. Baker, C. Combes, C. Rey, S. Sarda, A. J. Wright, M. E. Smith, J. V. Hanna, C. Gervais, D. Laurencin and C. Bonhomme, *Acta Biomater.*, 2016, **31**, 348–357.
- 14 C. Slater, D. Laurencin, V. Burnell, M. E. Smith, L. M. Grover, J. A. Hriljac and A. J. Wright, *J. Mater. Chem.*, 2011, **21**, 18783–18791.
- 15 A. P. Legrand, H. Sfihi, N. Lequeux and J. Lemaître, *J. Biomed. Mater. Res., Part B*, 2009, **91**, 46–54.
- 16 Y. Yu, H. Guo, M. Pujari-Palmer, B. Stevansson, J. Grins, H. Engqvist and M. Edén, *Ceram. Int.*, 2019, **45**, 20642–20655.
- 17 L. Mayen, N. D. Jensen, D. Laurencin, O. Marsan, C. Bonhomme, C. Gervais, M. E. Smith, C. Coelho, G. Laurent, J. Trebosc, Z. Gan, K. Chen, C. Rey, C. Combes and J. Soulié, *Acta Biomater.*, 2020, **103**, 333–345.
- 18 K. Momma and F. J. Izumi, *Appl. Crystallogr.*, 2011, **44**, 1272–1276.
- 19 G. Kresse and J. Hafner, *Phys. Rev. B: Condens. Matter Mater. Phys.*, 1994, **49**, 14251.
- 20 P. Giannozzi, S. Baroni, N. Bonini, M. Calandra, R. Car, C. Cavazzoni, D. Ceresoli, G. L. Chiarotti, M. Cococcioni, I. Dabo, A. Dal Corso, S. de Gironcoli, S. Fabris, G. Fratesi, R. Gebauer, U. Gerstmann, C. Gougoussis, A. Kokalj, M. Lazzeri, L. Martin-Samos, N. Marzari, F. Mauri, R. Mazzarello, S. Paolini, A. Pasquarello, L. Paulatto, C. Sbraccia, S. Scandolo, G. Sclauzero, A. P. Seitsonen, A. Smogunov, P. Umari and R. M. Wentzcovitch, *J. Phys.: Condens. Matter*, 2009, **21**, 395502.
- 21 S. Baroni, S. de Gironcoli, A. Dal Corso and P. Giannozzi, *Rev. Mod. Phys.*, 2001, **73**, 515–562.
- 22 J. P. Perdew, K. Burke and M. Ernzerhof, *Phys. Rev. Lett.*, 1996, **77**, 3865–3868.
- 23 N. Troullier and J. L. Martins, *Phys. Rev. B: Condens. Matter Mater. Phys.*, 1991, **43**, 1993–2006.
- 24 L. Kleinman and D. Bylander, *Phys. Rev. Lett.*, 1982, **48**, 1425–1428.
- 25 C. Pickard and F. Mauri, *Phys. Rev. B: Condens. Matter Mater. Phys.*, 2001, **63**, 245101.
- 26 K. Lejaeghere, G. Bihlmayer, T. Björkman, P. Blaha, S. Blügel, V. Blum, D. Caliste, I. E. Castelli, S. J. Clark, A. Dal Corso, S. de Gironcoli, T. Deutsch, J. Kay Dewhurst, I. Di Marco, C. Draxl, M. Dulak, O. Eriksson, J. A. Flores-Livas, K. F. Garrity, L. Genovese, P. Giannozzi, M. Giantomassi, S. Goedecker, X. Gonze, O. Grånäs, E. K. U. Gross, A. Gulans, F. Gygi, D. R. Hamann, P. J. Hasnip, N. A. W. Holzwarth, D. Iuşan, D. B. Jochym, F. Jollet, D. Jones, G. Kresse, K. Koepfner, E. Küçükbenli, Y. O. Kvashnin, I. L. M. Locht, S. Lubeck, M. Marsman, N. Marzari, U. Nitzsche, L. Nordström, T. Ozaki, L. Paulatto, C. J. Pickard, W. Poelmans, M. I. J. Probert, K. Refson, M. Richter, G.-M. Rignanese, S. Saha, M. Scheffler, M. Schlipf, K. Schwarz, S. Sharma, F. Tavazza, P. Thunström, A. Tkatchenko, M. Torrent, D. Vanderbilt, M. J. van Setten, V. Van Speybroeck, J. M. Wills, J. R. Yates, G.-X. Zhang and S. Cottenier, *Science*, 2016, **351**, aad3000.
- 27 C. Gervais, D. Laurencin, A. Wong, F. Pourpoint, J. Labram, B. Woodward, A. P. Howes, K. J. Pike, R. Dupree, F. Mauri, C. Bonhomme and M. E. Smith, *Chem. Phys. Lett.*, 2008, **464**, 42–48.
- 28 P. Pyykkö, *Mol. Phys.*, 2008, **106**, 1965.
- 29 K. M. N. Burgess, Y. Xu, M. C. Leclerc and D. L. Bryce, *Inorg. Chem.*, 2014, **53**, 552.
- 30 J. Bennazha, A. Boukhari and E. M. Holt, *Solid State Sci.*, 1999, **1**, 373–380.
- 31 L. Granasy, T. Pusztai, G. Tegze, J. Warren and J. Douglas, *Phys. Rev. A: At., Mol., Opt. Phys.*, 2005, **72**, 011605.
- 32 P. Gras, Etude physico-chimique et structurale de pyrophosphates de calcium hydratés: application aux microcalcifications associées à l'arthrose, *PhD thesis*, Université de Toulouse, France, 2014.
- 33 A. Rulmont, R. Cahay, M. Liegeois-Duyckaerts and P. Tarte, *Eur. J. Solid State Inorg. Chem.*, 1991, **28**, 207–219.
- 34 P. Gras, C. Rey, O. Marsan, S. Sarda and C. Combes, *Eur. J. Inorg. Chem.*, 2013, **34**, 5886–5895.
- 35 T. Balić-Žunić, M. R. Christoffersen and J. Christoffersen, *Acta Crystallogr., Sect. B: Struct. Sci.*, 2000, **56**, 953–958.
- 36 N. L. Davis, G. S. Mandel, N. S. Mandel and R. E. Dickerson, *J. Crystallogr. Spectrosc. Res.*, 1985, **15**, 513–521.
- 37 M. Harcharras, A. Ennaciri, A. Rulmont and G. Gilbert, *Spectrochim. Acta, Part A*, 1997, **53**, 345–352.
- 38 F. W. Poulsen, *J. Raman Spectrosc.*, 1986, **17**, 189–191.

## Supporting information

### Advances in the synthesis and structure of $\alpha$ -canaphite: a multitool and multiscale study

Laëtitia Mayen<sup>a</sup>, Nicholai D. Jensen<sup>b,c</sup>, Maximilien Desbord<sup>a</sup>, Danielle Laurencin<sup>b</sup>, Christel Gervais<sup>c</sup>, Christian Bonhomme<sup>c</sup>, Mark E. Smith<sup>d,e,f</sup>, Florence Porcher<sup>g</sup>, Erik Elkaim<sup>h</sup>, Cédric Charvillat<sup>a</sup>, Pierre Gras<sup>a</sup>, Christian Rey<sup>a</sup>, Jérémy Soulié<sup>a</sup>, Christèle Combes<sup>a,\*</sup>

<sup>a</sup>CIRIMAT, Université de Toulouse, CNRS, Toulouse INP - ENSIACET, Toulouse, France

<sup>b</sup>ICGM, Univ. Montpellier, CNRS, ENSCM, Montpellier, France

<sup>c</sup>Sorbonne Université, CNRS, Laboratoire de Chimie de la Matière Condensée de Paris, UMR 7574, Paris, France

<sup>d</sup>Vice-Chancellor's Office, Highfield Campus, University of Southampton, University Road, Southampton, SO17 1BJ, University of Southampton, UK, and Department of Chemistry, Lancaster University, Bailrigg, Lancaster, LA1 4YB, UK

<sup>e</sup>Department of Chemistry, Lancaster University, Bailrigg, Lancaster, LA1 4YB, UK

<sup>f</sup>Department of Physics, University of Warwick, CV47AL Coventry, UK

<sup>g</sup>Laboratoire Léon Brillouin, CEA Saclay, Gif-sur-Yvette, France

<sup>h</sup>Synchrotron Soleil, L'Orme les Merisiers, St Aubin, Gif-sur-Yvette, France

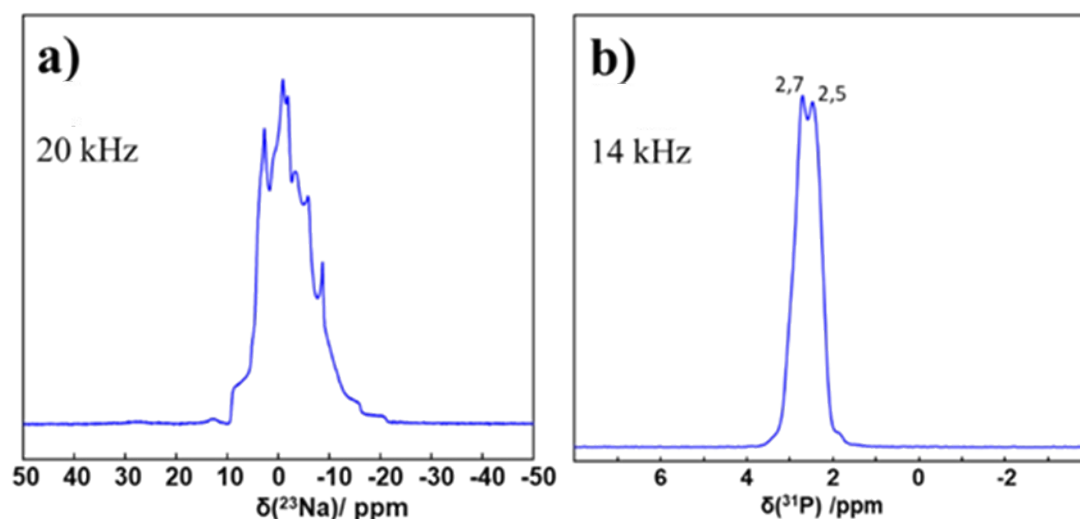


**Figure S1:** <sup>23</sup>Na (a) and <sup>31</sup>P (b) MAS NMR spectra at 14.1 T of the as-synthesized sodium pyrophosphate precursor ( $\text{Na}_4\text{P}_2\text{O}_7$ ) used to prepare  $\alpha$ -canaphite. Both NMR spectra are in agreement with published data for  $\text{Na}_4\text{P}_2\text{O}_7$  (four sites for Na and two sites for P) and confirmed the purity of the sodium and pyrophosphate precursor salt.<sup>1-2</sup>

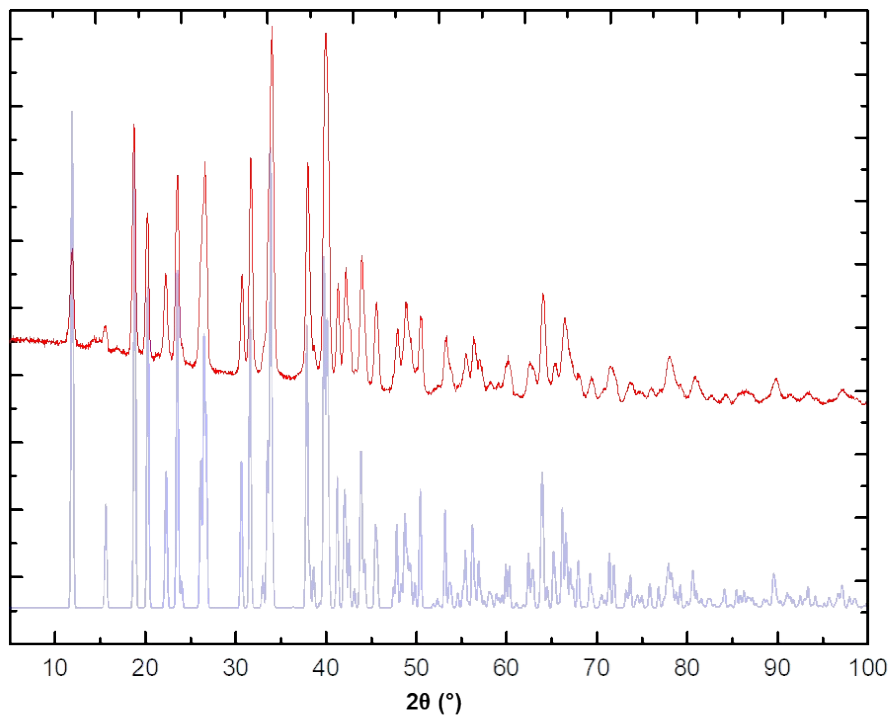


**Figure S2:** X-ray pattern of the as-synthesized  $\alpha$ -canaphite powder obtained with the laboratory X-ray diffractometer ( $\lambda_{\text{Co}(K\alpha)} = 1.788970 \text{ \AA}$ ) (in red) compared to that for a synthetic canaphite monocrystal<sup>8</sup> (ICSD n°26015) (in blue).

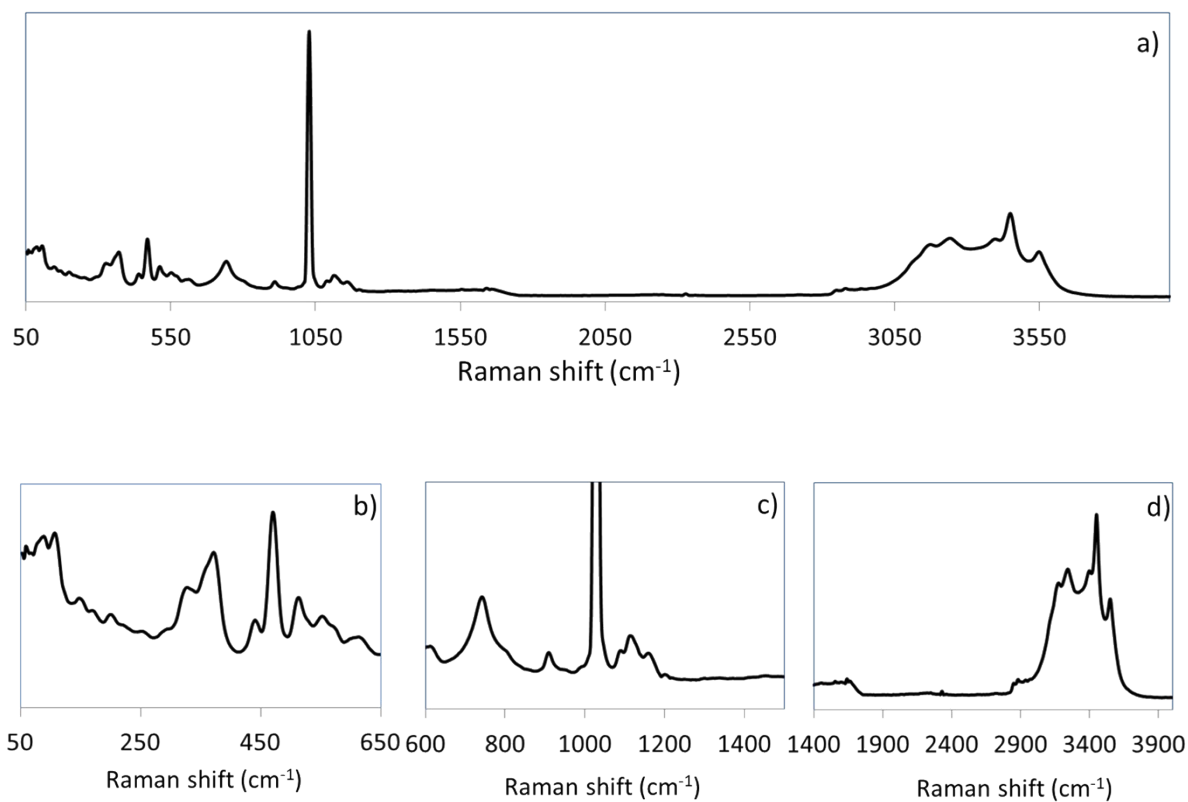


**Figure S3:** Raman spectrum of the  $\alpha$ -canaphite powder synthesized in H<sub>2</sub>O: full spectrum (a) and spectrum divided in three separated domains (b, c and d). The positions and assignments of the lines are reported in Table S4.

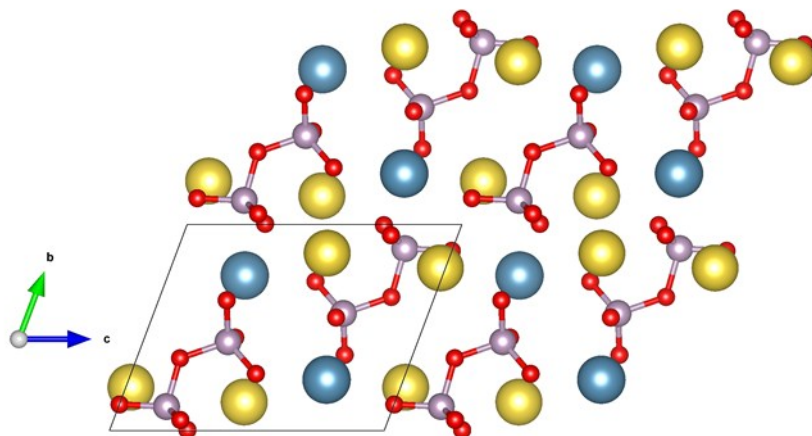


**Figure S4:** Three-dimensional representation of the triclinic elemental cell of the anhydrous calcium disodium pyrophosphate ( $\alpha$ - $\text{CaNa}_2\text{P}_2\text{O}_7$ ). (yellow: sodium, blue: calcium, grey: phosphorus, red: oxygen)

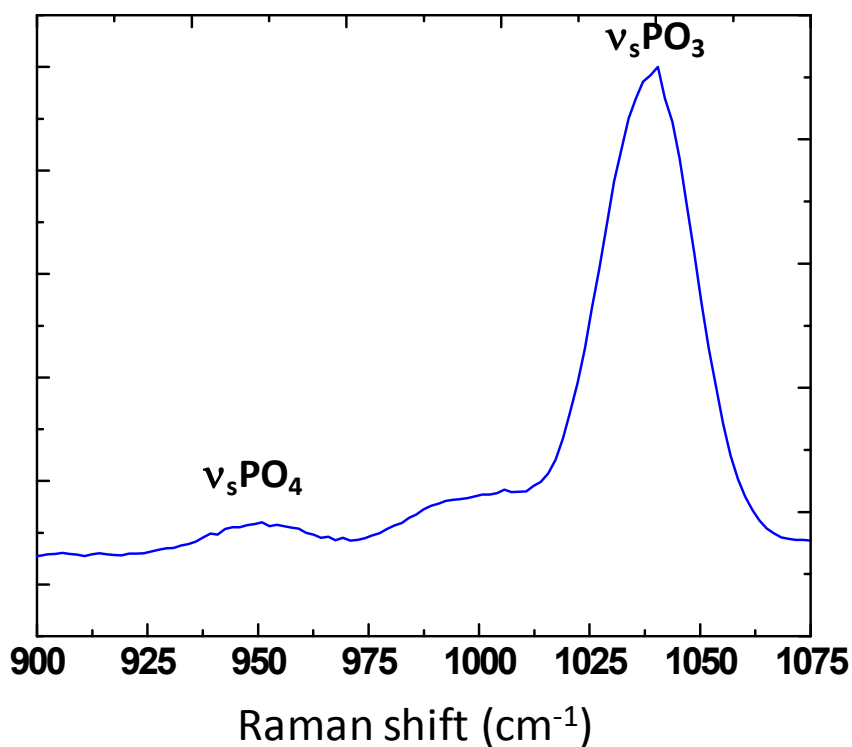


**Figure S5:** Raman spectrum (900-1075  $\text{cm}^{-1}$  domain) of  $\alpha$ -canaphite dried at  $250^\circ\text{C}$  showing the presence of a weak characteristic vibration band of the orthophosphate group  $\nu_s\text{PO}_4$  in addition to the strong  $\nu_s\text{PO}_3$  band of pyrophosphate testifying for an internal hydrolysis of part of pyrophosphate ions into orthophosphate ones according to the equation:  $\text{P}_2\text{O}_7^{4-} + \text{H}_2\text{O} \rightarrow 2 \text{HPO}_4^{2-}$ .



**Table S1:** Structural parameters and symmetry of  $\alpha$ -CaNa<sub>2</sub>P<sub>2</sub>O<sub>7</sub> determined by XRD analysis on single crystal<sup>29</sup> compared to the refinement data (Rietveld refinement on laboratory X-ray diffraction data) of the  $\alpha$ -CaNa<sub>2</sub>P<sub>2</sub>O<sub>7</sub> powder obtained after the heat treatment at 400°C during 15 h of the synthesized  $\alpha$ -canaphite.

$\alpha$ -CaNa <sub>2</sub> P <sub>2</sub> O <sub>7</sub> sample	Symmetry	Volume (Å <sup>3</sup> )	a (Å)	b (Å)	c (Å)	$\alpha$ (°)	$\beta$ (°)	$\gamma$ (°)
Monocrystal (Bennazha 1999)	Triclinic	308.5(3)	5.361(3)	7.029(3)	8.743(4)	69.40(2)	89.02(3)	88.78(4)
As-synthesized powder	Triclinic	316.852 (68)	5.40070 (65)	7.09929 (88)	8.8295(11)	69.4248 (22)	89.0318 (33)	88.7703 (22)

### Supporting Information on Vibrational Spectroscopy:

Considering the crystal structure of  $\alpha$ -canaphite, the factor group is Cs and the primitive unit cell contains two chemical formula units. The complete treatment results in:

- Acoustic mode (corresponding to crystal vibrations):  $2 A' \oplus A''$
- External vibrations:  $22 A' \oplus 23 A''$
- Librations  $15 A' \oplus 15 A''$  ( $3 A' \oplus 3 A''$  for  $P_2O_7^{4-}$  and  $12 A' \oplus 12 A''$  for  $H_2O$ )
- Internal vibrations of  $P_2O_7^{4-}$  ( $21 A' \oplus 21 A''$ ) and  $H_2O$  ( $12 A' \oplus 12 A''$ )

Considering the  $P_2O_7^{4-}$  molecular unit, the correlation table (Table S2) indicates the distribution of the internal vibrations relative to the original free ion vibratory domains. The 42 total internal vibrations both active in infrared and Raman spectroscopies, are associated to doubling of the vibration levels of the initial free ion. The correlation table for water molecules is reported in Table S3. The 24 total internal vibrations correspond to a multiplication by 8 of the vibration levels of the original molecule. It shall be considered that additional lines corresponding to libration movements of water molecules may possibly occur in the  $P_2O_7^{4-}$  vibration range. Lattice vibrations show up at low energies and have not been considered in this MIR analysis.

**Table S2:** Correlation table for  $P_2O_7^{4-}$

Symmetry of free $P_2O_7^{4-}$ ion $C_{2v}$	Site symmetry (for each $P_2O_7^{4-}$ ion) $C_1$	Factor group (2 $P_2O_7^{4-}$ ) $C_s$
7 $A_1$ (IR, Raman)	21 A	7 $A' \oplus 7 A''$ (IR, Raman)
4 $A_2$ (Raman)		4 $A' \oplus 4 A''$ (IR, Raman)
6 $B_1$ (IR, Raman)		6 $A' \oplus 6 A''$ (IR, Raman)
4 $B_2$ (IR, Raman)		4 $A' \oplus 4 A''$ (IR, Raman)

**Table S3:** Correlation table for  $H_2O$  ( $D_2O$ )

Symmetry of free molecule $C_{2v}$	Site symmetry (for each water molecule) $C_1$	Factor group (8 $H_2O$ ) $C_s$
2 $A_1$ (IR, Raman)	3 A	8 $A' \oplus 8 A''$ (IR, Raman)
$B_1$ (IR, Raman)		4 $A' \oplus 4 A''$ (IR, Raman)

For libration modes of water molecules the factor group treatment predicts  $12 A' \oplus 12 A''$  (IR, Raman).

**Table S4:** FTIR and Raman spectral lines of  $\alpha$ -canaphite and its deuterated analogue (corresponding to the Figure 9): position ( $\text{cm}^{-1}$ ), intensity and assignments.

Assignments	H <sub>2</sub> O-canaphite		D <sub>2</sub> O-canaphite		
	FTIR	Raman	FTIR	Raman	
v <sub>s</sub> and v <sub>as</sub> H <sub>2</sub> O (D <sub>2</sub> O)	3562 m	3550 m	2633 m	2627 m	
	3501 sh		2563 sh		
	3454 m	3450 m	2549 m	2555 m	
	3392 w	3399 m	2521 w	2522 w	
	3335 vw		2431 m	2438 sh	
				2401 sh	
	3241 m	3241 m	2378 m		
	3169 w	3173 w	2355 sh	2359 m	
	3116 sh		2337 sh		
$\delta$ H <sub>2</sub> O (D <sub>2</sub> O)	1658 b m	1650 bw	1213 sh	1221 b	
v <sub>s</sub> and v <sub>as</sub> PO <sub>3</sub>	1157 sh	1160 w		1160 w	
	1139 s		1137 s		
	1125 sh	1126 sh	1124 sh	1128 sh	
	1108 m	1114 w	1108 m	1113 w	
	1090 s	1090 w	1089 s	1092 w	
	1032 sh				
	1027 m	1028 vs	1028 m	1029 vs	
	991 w	990 vw	991 w		
	938 m		934 m		
$\delta$ P <sub>2</sub> O <sub>7</sub> , external modes	v <sub>as</sub> POP	909 m	908 w	906 w	908 w
	v <sub>L</sub> H <sub>2</sub> O	797 b w	800 b sh	791 sh	
	v <sub>s</sub> POP		743 m	740 w	742 m
	v <sub>L</sub> H <sub>2</sub> O	706 b m		705 b w	
		614 w	609 w	617 sh	620 w
				606 sh	
		569 sh	569 sh	570 m	573 w
	v <sub>L</sub> H <sub>2</sub> O	550 m	552 w		
		510 vw	512 w	503 sh	527 w
		468 w	470 m	472 w	470 m
		438 vw	440 w		427 w

b: broad, m: medium intensity, sh: shoulder, v: very, s: strong, w: weak,  
v<sub>s</sub> and v<sub>as</sub>: symmetric and antisymmetric stretching, v<sub>L</sub>: water libration line,  $\delta$ : bending

## References

- 1 L. Griffiths, A. Root, R. K. Harris, K. J. Packer and F. R. Tromans, *J. Chem. Soc. Dalton Trans*, 1986, **10**, 2247–2251.
- 2 S. Hayashi and K. Hayamizu, *Chemical Physics*, 1991, **157**, 381–389.